

Integrable 2D Lorentzian Gravity and Random Walks

P. Di Francesco¹, E. Guitter²

*CEA-Saclay, Service de Physique Théorique,
F-91191 Gif sur Yvette Cedex, France*

C. Kristjansen³

*The Niels Bohr Institute,
Blegdamsvej 17, DK-2100 Copenhagen Ø, Denmark*

We introduce and solve a family of discrete models of 2D Lorentzian gravity with higher curvature weight, which possess mutually commuting transfer matrices, and whose spectral parameter interpolates between flat and curved space-times. We further establish a one-to-one correspondence between Lorentzian triangulations and directed Random Walks. This gives a simple explanation why the Lorentzian triangulations have fractal dimension 2 and why the curvature model lies in the universality class of pure Lorentzian gravity. We also study integrable generalizations of the curvature model with arbitrary polygonal tiles. All of them are found to lie in the same universality class.

07/99

¹ philippe@spht.saclay.cea.fr, partially supported by NSF grant PHY-9722060

² guttter@spht.saclay.cea.fr

³ kristjan@alf.nbi.dk, supported by the Carlsberg Foundation

1. Introduction

The invention of a transfer matrix technique for dynamical triangulations [1,2] has made it possible to introduce a concept of distance in two-dimensional quantum gravity. This again has made it possible, in the case of pure gravity, to calculate analytically a loop-loop correlation function as a function of geodesic distance and to show that the scaling relations from flat space statistical mechanics have analogues in the quantum theory [3]. An intriguing result of these investigations is that the fractal dimension of the quantum space times turns out to be four and not two. Unfortunately, when it comes to the inclusion of matter fields the transfer matrix technique for dynamical triangulations has not yet proven as efficient as its regular lattice counterpart. Correlators as a function of geodesic distance have been studied numerically [4–7] but analytical calculations have not been possible.⁴

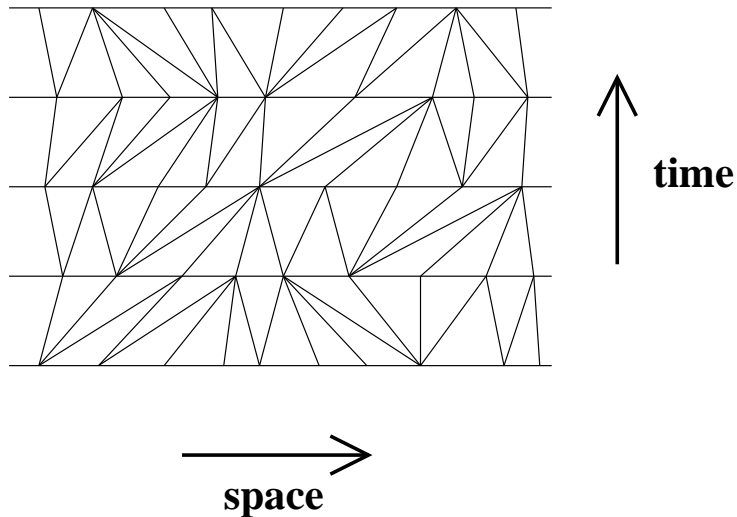


Fig. 1: A typical discretized universe of $(1+1)$ -dimensional Lorentzian quantum gravity. Each constant-time strip is an arbitrary succession of triangles pointing up or down. Boundary conditions can be chosen to be periodic, free, fixed according to the model at hand.

Recently, a different discrete approach to two-dimensional quantum gravity has been proposed [12,13]. In this approach which is known as Lorentzian quantum gravity only triangulations which admit a causal structure are allowed in the state sum. An example of such a triangulation is shown in Fig. 1. The elementary building blocks are triangles with one space-like and two time-like edges which are glued together at random so as to form

⁴ There have, however, been such calculations using an alternative, fully valid, but not equivalent definition of distance [8–10], see also [11].

a piling of constant-time slices. In a sense such triangulations represent only the space fluctuations of the universe while respecting chronology. In Lorentzian quantum gravity, baby universes are not allowed. In other words, a given time slice of the triangulation has only one connected component. This, in particular, means that a universe always has spherical topology. The model of pure Lorentzian quantum gravity was solved in [12] exploiting the fact that the generating functional for its transfer matrix obeyed a certain iterative equation. The continuum limit of the model proved to be different from that of usual Euclidean quantum gravity or Liouville theory. For instance, the fractal dimension of the quantum universes turned out to be equal to two. However, the continuum limit of Lorentzian quantum gravity is in accordance with continuum results obtained from calculations carried out in the proper time gauge [14].⁵ A Lorentzian lattice by construction is something between a regular lattice and a truly random one. It is therefore interesting to know if the introduction of matter fields on such lattices leads to any interaction between matter and geometry. In [15] the effect of coupling an Ising model to Lorentzian quantum gravity was studied. The investigations were based partly on a high temperature expansion, partly on Monte Carlo simulations. No sign of interaction between matter and geometry was seen. Numerical simulations currently being carried out indicate, however, that for matter fields with $c > 1$ a non-trivial interaction between matter and geometry takes place [16].

In a first part of the present article we formulate and solve exactly various other extensions of two-dimensional Lorentzian quantum gravity. The simplest extension, which we develop in details throughout the paper, is that of Lorentzian gravity with a higher curvature term which is equivalent to Lorentzian quantum gravity coupled to a simple dimer model or to Lorentzian quantum gravity with universes built from triangles and squares. We show that this model is integrable in the sense that its transfer matrix can be explicitly diagonalized and that there exists a set of commuting transfer matrices which allow us to interpolate between regular and random Lorentzian lattices. Furthermore we describe how to construct models of Lorentzian quantum gravity allowing general p -gons as building blocks while preserving the integrability structure. As will become evident the transfer matrix formulation is by far more efficient for Lorentzian than for Euclidean triangulations. In fact the integrability structure revealed has many treats in common

⁵ If baby universes are allowed in Lorentzian quantum gravity the usual Euclidean gravity continuum limit is obtained. We refer to [12] for a discussion of this point.

with the integrability structure found in regular lattice transfer matrix studies and it is our hope that our further investigation of this structure will enable us to solve exactly more realistic systems of matter fields coupled to Lorentzian quantum gravity such as Lorentzian triangulations equipped with Ising spins. For all the models that we have considered so far the universality class of the geometrical system is the same as that of pure Lorentzian quantum gravity.

In a second part of this article we study the relationship between Lorentzian quantum gravity and random walks. We prove that there exists a one-to-one correspondence between Lorentzian triangulations and directed random walks drawn on the regular triangular lattice. This allows us to set up a dictionary connecting concepts in Lorentzian quantum gravity to concepts in the theory of random walks. For instance, the expression for the loop-loop correlation function follows from a similar expression for large excursion probabilities for random walks. Furthermore, the integrability structure of the model of Lorentzian quantum gravity with a higher curvature term can be understood in terms of the possibility of a simple block decomposition of the corresponding random walk. Finally the random walk equivalence provides an explanation why Lorentzian triangulations have fractal dimension two and why we can not obtain from our model with a higher curvature term other critical behaviour than that of pure Lorentzian quantum gravity.⁶

The simple extension of Lorentzian quantum gravity involving a higher curvature term as well as its various alternative interpretations are described in Sect. 2. Sect. 3 treats the equivalence between random walks and Lorentzian triangulations and Sect. 4 contains a discussion of Lorentzian gravity involving general polygonal building blocks. Finally, in Sect. 5 we conclude and discuss the future prospects of transfer matrix techniques for Lorentzian triangulations.

2. Discrete Lorentzian 2D Gravity via Triangulations

2.1. Lorentzian Quantum Gravity with a Higher Curvature Term

We consider quantum universes of the type depicted in Fig. 1. Generally we will be interested in a time evolution from, say, time $t = 1$ to $t = T$, i.e. a time strip of width T .

⁶ Dimensional analysis indicates that adding a higher curvature term to the Einstein-Hilbert action should not modify continuum physics. However, this argument is only valid perturbatively and one could still hope for the existence of a (non-perturbative) ultra-violet fixed point, a scenario (in 4D) denoted by Weinberg as asymptotic safety [17].

In the course of the article we will consider various possible boundary conditions in space. These will be explained at the relevant points.

As usual in two-dimensional gravity, we will attach a weight g per triangular face, resulting in an overall factor of g^A for each triangulation, where A is the total number of triangles, measuring the area if we decide that triangles have unit area.

We now generalize the model by also attaching to each triangulation an intrinsic curvature weight defined as follows. For a two-dimensional triangulated manifold, curvature resides on vertices, and the curvature at a vertex is proportional to $(v - 6)$ where v is the valence of the vertex. Here we do not wish to add an ordinary curvature term (which is trivial in two dimensions) but a term which suppresses (or enforces) local curvature. Due to the time slice structure of the triangulation we take as a measure of the curvature at a vertex the quantity $|v_1 - 3| + |v_2 - 3|$ where v_1 and v_2 are the number of triangles adjacent to the vertex in the upper and the lower time-slice respectively, and we attach to each vertex of the triangulation the weight $a^{(|v_1-3|+|v_2-3|)/2}$. Introducing this weight factor can be viewed as adding a higher curvature term to the Einstein-Hilbert action (note, however, that one can have $v - 6 = 0$ and $|v_1 - 3| + |v_2 - 3| \neq 0$). Our model is similar in spirit to the models considered in [18], where the effect of adding a higher curvature term to usual dynamically triangulated gravity was considered. Since any vertex is linked to exactly two up (resp. down) triangles in its upper (resp. lower) slice, with an arbitrary number of down (resp. up) triangles in-between, a simpler, completely equivalent way to introduce the curvature weight is to attach a weight a per *pair* of adjacent triangles pointing both up or both down, within the same constant-time slice. The graphical representation of Fig.1 is more transparent in the dual picture, where a constant-time strip becomes a succession of half-edges attached to the dual constant-time line, where the half-edges lying above (resp. below) the line correspond to triangles pointing down (resp. up). Moreover, as each triangle has exactly one space-like edge, the triangles pointing down in the strip of time t all share an edge with the triangles pointing up in the strip of time $t + 1$, henceforth the dual half-edges are connected to form edges between the lines of time t and $t + 1$.

The Boltzmann weights defined above are depicted in Fig.2, where we also give an example of a world-sheet configuration in the dual picture.

The Lorentzian gravity problem above, and its generalization with intrinsic curvature admit a transfer matrix formulation. Indeed, if we compute the Boltzmann weight of a single time-line with i lower half-edges and j upper ones, and sum over all possible relative positions of these half-edges, we find a number $T_{i,j}(g, a)$ that depends only on the numbers

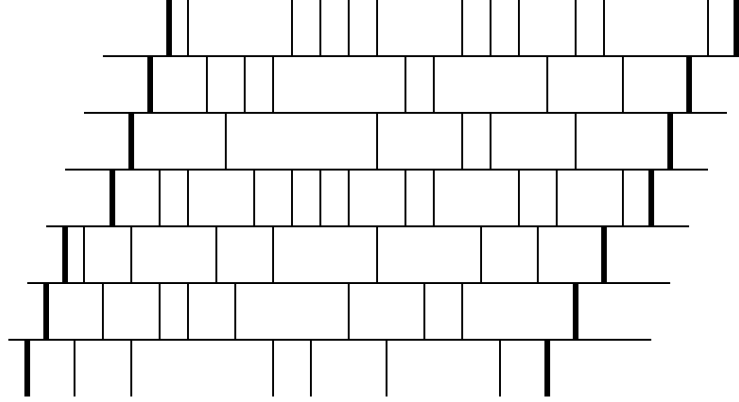
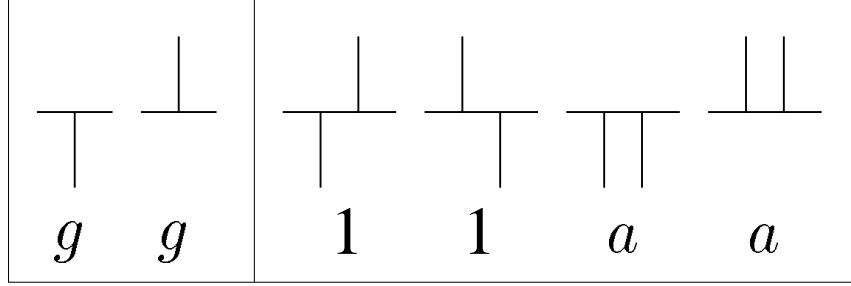


Fig. 2: The Boltzmann weights of the Lorentzian gravity model with a higher curvature term. Each vertex (of the dual lattice) receives a factor g . In addition each sequence of neighbouring up-up or down-down half-edges receives a factor a . We have represented a typical world-sheet configuration.

of half-edges, but not on their specific relative positions. This can in turn be taken as the transfer matrix element (i, j) , that transfers from a row of i half-edges to one of j . For instance, the partition function of a strip of time width T , with ℓ_1 lower triangles pointing up and ℓ_2 upper ones pointing down is simply

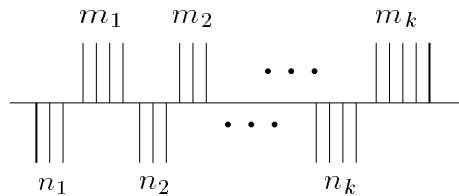
$$Z_{\ell_1, \ell_2}(T|g, a) = \left(T(g, a)^T \right)_{\ell_1, \ell_2}. \quad (2.1)$$

For periodic boundary conditions, this is the so-called two-loop correlator of Lorentzian gravity, which describes world sheets of cylindric form bounded by two loops of respective lengths ℓ_1 and ℓ_2 .

Let us adopt the following choice of fixed boundary conditions, that differ from the periodic ones of [13]. We assume that each time strip always has one lower half-edge (i.e. triangle pointing up) on its leftmost end and one upper one (triangle pointing down) on its rightmost end. This implies in particular that $i, j \geq 1$ in the transfer matrix, i.e. that the time slices never degenerate into the vacuum. These boundary conditions can be

described as “staircase” conditions since they imply that the left and right hand side space-like boundaries of the world-sheet have the shape of a staircase with the stairs extending to the right at each successive time line (see the example of Fig.2). For reasons that will become clear later, we attach a weight \sqrt{g} only to each of the two *boundary* half-edges in each slice.

We may now compute the transfer matrix element $T_{i,j}(g, a)$ by summing over all possible configurations of upper and lower half-edges. This is done by first summing over the number $k \geq 1$ of blocks made, say, of $n_r \geq 1$ consecutive lower half-edges, followed by $m_r \geq 1$ upper ones, $r = 1, 2, \dots, k$, and then summing over the corresponding partitions of $i = \sum_r n_r$ and $j = \sum_r m_r$, with positive integers n_r, m_r . Note that the conditions $n_1 \geq 1$ and $m_k \geq 1$ are a direct consequence of the boundary conditions we have imposed. We get

$$\begin{aligned}
T_{i,j}(g, a) &= \sum_{k \geq 1} \sum_{\substack{n_r, m_r \geq 1, \\ \sum n_r = i, \sum m_r = j}} \sum_{r=1,2,\dots,k} \\
&= \sum_{k \geq 1} \sum_{\substack{n_r, m_r \geq 1, \\ \sum n_r = i, \sum m_r = j}} g^{i+j-1} a^{\sum(n_r-1) + \sum(m_r-1)} \\
&= g^{i+j-1} a^{i+j} \sum_{k \geq 1} \frac{1}{a^{2k}} \binom{i-1}{k-1} \binom{j-1}{k-1}.
\end{aligned}
\tag{2.2}$$


This is in general a polynomial of a , as the range of the summation is finite ($k \leq \min(i, j)$).

The formula (2.2) is best encapsulated into the generating function

$$\begin{aligned}
\theta(x, y|g, a) &= \sum_{i,j \geq 1} x^i y^j T_{i,j}(g, a) \\
&= \frac{1}{g} \sum_{k \geq 1} \frac{1}{a^{2k}} \sum_{i \geq k} \binom{i-1}{k-1} (gax)^i \sum_{j \geq k} \binom{j-1}{k-1} (gay)^j \\
&= \frac{1}{g} \sum_{k \geq 1} \frac{1}{a^{2k}} \frac{(gax)^k (gay)^k}{(1-gax)^k (1-gay)^k} \\
&= \frac{gxy}{1-ga(x+y) - g^2(1-a^2)xy}.
\end{aligned}
\tag{2.3}$$

In the particular case $a = 1$, this reduces to the generating function for pure Lorentzian gravity discretized via triangulations to be compared with that of [12], but with different boundary conditions. When $a = 0$, (2.3) reduces to the generating function for flat world-sheets. Indeed, $\theta(x, y|g, 0) = gxy/(1 - g^2xy)$ simply means that $T_{i,j}(g, 0) = g^{i+j-1} \delta_{i,j}$.

In other words, the pattern of triangles becomes regular (successions of triangles pointing up,down,up,...etc...), and the discrete world-sheet becomes a rhombus-shaped portion of the triangular lattice, with area $2\ell \times T$, where ℓ denotes the number of lower triangles pointing up in the first time slice. Hence our parameter a allows us to interpolate between flat and curved spaces.

2.2. Diagonalization of the transfer matrix

To solve our model, and be able to compute quantities like (2.1), the simplest strategy is to diagonalize the transfer matrix $T(g, a)$. But as the number of triangles in each time slice is not bounded, the matrix has infinite size. Nevertheless, at the expense of extra precautions, we have been able to construct a complete set of orthonormal eigenvectors for $T(g, a)$, as a linear map acting on the infinite-dimensional vector space $E = \mathbb{R} \otimes \mathbb{R} \otimes \dots$. They read as follows.

Unless otherwise noted, we will always assume that the parameters g and a are real and satisfy the inequalities

$$\left| \frac{1 - g^2(1 - a^2)}{ga} \right| > 2, \quad |ga| < 1. \quad (2.4)$$

Let $q \equiv q(g, a)$ be the real solution to the quadratic equation

$$ga\left(q + \frac{1}{q}\right) = 1 - g^2(1 - a^2), \quad (2.5)$$

such that $|q| < 1$. Then the functions

$$\begin{aligned} F_m(x|q) &= \sum_{i \geq 1} x^i v_i^{(m)}(q) \\ &= \sqrt{1 - q^2} \frac{x(q - x)^{m-1}}{(1 - qx)^m}, \end{aligned} \quad (2.6)$$

for $m = 1, 2, 3, \dots$ are the generating functions for the components $v_i^{(m)}$ of the m -th eigenvector $v^{(m)} \equiv v^{(m)}(g, a)$ for $T(g, a)$. Moreover the corresponding vectors form an orthonormal basis of E .

The second statement is readily proved by considering the following contour integral over the unit circle

$$\begin{aligned}
v^{(m+p)} \cdot v^{(m)} &= \sum_{i \geq 1} v_i^{(m+p)} v_i^{(m)} \\
&= \oint \frac{dx}{2i\pi x} F_{m+p}(x|q) F_m\left(\frac{1}{x}|q\right) \\
&= -(1-q^2) \oint \frac{dx}{2i\pi} \frac{(q-x)^{p-1}}{(1-qx)^{p+1}} \\
&= \begin{cases} 0 & \text{if } p \geq 1 \\ 1 & \text{if } p = 0 \end{cases}
\end{aligned} \tag{2.7}$$

where, using the Cauchy residue formula, we have noted that there was no pole of the integrand inside the unit disc when $p \geq 1$ (recall that $|q| < 1$), and the result for $p = 0$ is simply given by the residue at the pole $x = q$. This proves the orthonormality of the set of vectors $\{v^{(m)}\}_{m=1,2,\dots}$. It is also easy to see that the matrix V with entries $V_{i,m} = v_i^{(m)}$ is symmetric. This is proved by noting that the generating function

$$v(x, y|q) = \sum_{i,m \geq 1} x^i y^m v_i^{(m)} = \frac{\sqrt{1-q^2} xy}{1 - q(x+y) + xy}, \tag{2.8}$$

is manifestly symmetric in x and y . From this symmetry and the orthogonality relation (2.7), we deduce the following completeness relation

$$\sum_{m \geq 1} v_i^{(m)} v_j^{(m)} = \delta_{ij}. \tag{2.9}$$

The first statement above, that $v^{(m)}$ be the m -th eigenvector of $T(g, a)$, is proved analogously, by means of a contour integral over the unit circle:

$$\begin{aligned}
\sum_{i \geq 1} x^i \left(T(g, a) v^{(m)} \right)_i &= \sum_{i,j \geq 1} x^i T_{i,j}(g, a) v_j^{(m)} \\
&= \oint \frac{dy}{2i\pi y} \theta(x, y|g, a) F_m\left(\frac{1}{y}|q\right) \\
&= \sqrt{1-q^2} \oint \frac{dy}{2i\pi y} \frac{gxy}{(1-gax) - y(ga + g^2(1-a^2)x)} \frac{\frac{1}{y}(q - \frac{1}{y})^{m-1}}{(1 - \frac{q}{y})^m} \\
&= \frac{gx}{ga + g^2(1-a^2)x} F_m\left(\frac{ga + g^2(1-a^2)x}{1-gax} | q\right) \\
&= \sqrt{1-q^2} gx \frac{\left((1-gax)q - (ga + g^2(1-a^2)x)\right)^{m-1}}{(1-gax - q(ga + g^2(1-a^2)x))^m}.
\end{aligned} \tag{2.10}$$

Note that only the pole $y = y_0(x) = (1 - gax)/(ga + g^2(1 - a^2)x)$ has contributed to the contour integral, as we have taken now only the poles lying *outside* the unit disc, and $y_0(x) > 1$ for $|x| < 1$, thanks to the inequalities (2.4). Using the equation (2.5), we may write $g^2(1 - a^2) = 1 - ag(q + \frac{1}{q})$, and notice that the numerator and denominator monomials in the last line of (2.10) respectively read

$$\begin{aligned} (1 - gax)q - (ga + g^2(1 - a^2)x) &= (q - x)\left(1 - \frac{ga}{q}\right), \\ 1 - gax - q(ga + g^2(1 - a^2)x) &= (1 - qx)(1 - qga), \end{aligned} \quad (2.11)$$

so that we finally arrive at the eigenvalue equation

$$T(g, a)v^{(m)} = \Lambda_m v^{(m)}, \quad (2.12)$$

where

$$\Lambda_m \equiv \Lambda_m(g, a) = g \frac{\left(1 - \frac{ga}{q}\right)^{m-1}}{(1 - qga)^m}, \quad (2.13)$$

for $m = 1, 2, 3, \dots$

Let us examine our result in the pure Lorentzian gravity case $a = 1$. The quadratic equation (2.5) is solved as

$$q(g, 1) = gC(g^2), \quad (2.14)$$

for $|g| < \frac{1}{2}$, where

$$C(x) = \frac{1 - \sqrt{1 - 4x}}{2x} = \sum_{n \geq 0} \frac{(2n)!}{(n+1)!n!} x^n, \quad (2.15)$$

is the generating function of the Catalan numbers, satisfying $xC^2(x) = C(x) - 1$. The eigenvalues can then be simplified to read

$$\Lambda_m = [gC(g^2)]^{2m-1} = q^{2m-1}. \quad (2.16)$$

Note that as $|q| < 1$, we have $\Lambda_1 > \Lambda_2 > \dots > 0$, and all the eigenvalues have series expansions in powers of g with positive integer coefficients.

2.3. Commuting transfer matrices

We now make the crucial observation that the eigenvectors $v^{(m)}(g, a)$ of the previous section only depend on q , which is itself a certain function of g and a . Hence there exists an infinite family of matrices $T(g, a)$ sharing the same eigenvectors, namely those for which the values of g, a lead to the same value of q . But matrices which can be diagonalized simultaneously form a commuting set. More precisely, the following statement holds:

$$[T(g, a), T(g', a')] = 0 \quad \text{iff} \quad \frac{1 - g^2(1 - a^2)}{ga} = \frac{1 - (g')^2(1 - (a')^2)}{g'a'} = q + \frac{1}{q}, \quad (2.17)$$

for arbitrary q (assumed to be real and such that $|q| < 1$). Moreover, the common eigenvectors are given by (2.6). Again, Eq.(2.17) can be proved directly by use of contour integrals involving the product of two generating functions (2.3).

To better understand the mechanism of this commutation, let us express the transfer matrix T in terms of its orthonormal eigenvectors and of its eigenvalues, namely

$$\begin{aligned} \theta(x, y|g, a) &= \sum_{m \geq 1} F_m(x|q) \Lambda_m F_m(y|q) \\ &= \frac{g}{1 - qga} \sum_{m \geq 1} F_m(x|q) \lambda^{m-1} F_m(y|q) \\ &= \sqrt{\lambda} \sum_{m \geq 1} F_m(x|q) \lambda^{m-1} F_m(y|q), \end{aligned} \quad (2.18)$$

where we have identified

$$\lambda = \frac{1 - \frac{ga}{q}}{1 - qga}, \quad (2.19)$$

by use of (2.13). For any fixed q with $|q| < 1$, we may use the (spectral) parameter λ to characterize the different commuting matrices (2.17). Denoting

$$T_q(\lambda) = T(g, a) \quad \text{for} \quad \frac{1 - g^2(1 - a^2)}{ga} = q + \frac{1}{q} \quad \text{and} \quad ga = \frac{1 - \lambda}{\frac{1}{q} - q\lambda}, \quad (2.20)$$

and

$$V_q^{(m)} = v^{(m)}(g, a), \quad (2.21)$$

independently of λ , we have from (2.18)

$$T_q(\lambda) = \sqrt{\lambda} \sum_{m \geq 1} \lambda^{m-1} V_q^{(m)} (V_q^{(m)})^t, \quad (2.22)$$

where we have used the orthogonal projector $P_q^{(m)} \equiv V_q^{(m)}(V_q^{(m)})^t$ onto the m -th eigenspace of $T_q(\lambda)$. Thanks to the orthogonality relation for the eigenvectors, which translates into $P_q^{(m)}P_q^{(m')} = \delta_{m,m'}P_q^{(m)}$, we easily get that

$$T_q(\lambda)T_q(\lambda') = T_q(\lambda\lambda'). \quad (2.23)$$

This relation trivially implies the commutation of transfer matrices (2.17). But this is a much stronger constraint. Note that all real values of λ and q such that $|q| < 1$ are allowed. Note also that both the commutation (2.17) and the multiplicativity property of spectral parameters (2.23) hold only with the help of the curvature weight a . The “solvability” of the case without a curvature term (allowing for the solution of [12]) is simply a consequence of these more general properties. Finally, let us mention that the transfer matrix of the regular lattice is a member of the family indexed by the parameter q for *any* q , as it can be obtained by taking the limit $a \rightarrow 0$, $g \rightarrow 1$ while keeping the ratio $(1 - g^2(1 - a^2))/(ga) = q + (1/q)$ fixed. In this limiting case, $\lambda = 1$ and the transfer matrix $T_q(1)$ is nothing but the identity matrix.

To conclude this section, let us rewrite the generating function (2.3) in terms of q and λ only

$$\begin{aligned} \theta_q(x, y|\lambda) &= \sum_{i,j \geq 1} x^i y^j [T_q(\lambda)]_{i,j} \\ &= \frac{\sqrt{\lambda}xy(1 - q^2)}{(1 - qx)(1 - qy) - \lambda(q - x)(q - y)}. \end{aligned} \quad (2.24)$$

2.4. Squares and Triangles

The curvature model introduced above may be reinterpreted as a discrete model for Lorentzian gravity, where the world-sheet is generated by arbitrary tessellations with squares and triangles that respect chronology. This is easily seen by performing the following transformation on the configurations of the previous model.

Let us expand again in powers of x and y the generating function (2.3)

$$\theta(x, y|g, a) = \frac{gxy}{1 - ga(x + y) - g^2(1 - a^2)xy}. \quad (2.25)$$

and interpret each contribution to $x^i y^j$ as a configuration of i lower and j upper half-edges. By expanding the denominator of (2.25), we get an arbitrary sequence of terms gax , gay or $g^2(1 - a^2)xy$. Whenever a term gax (resp. gay) is picked, we interpret it as an isolated lower (resp. upper) half edge, which comes with a weight ga . Whenever a term $g^2(1 - a^2)xy$

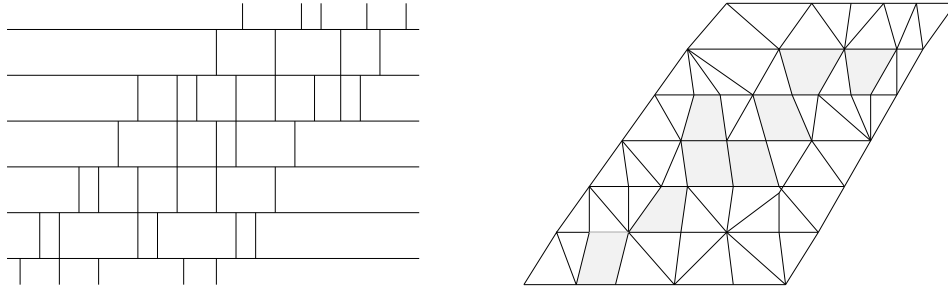
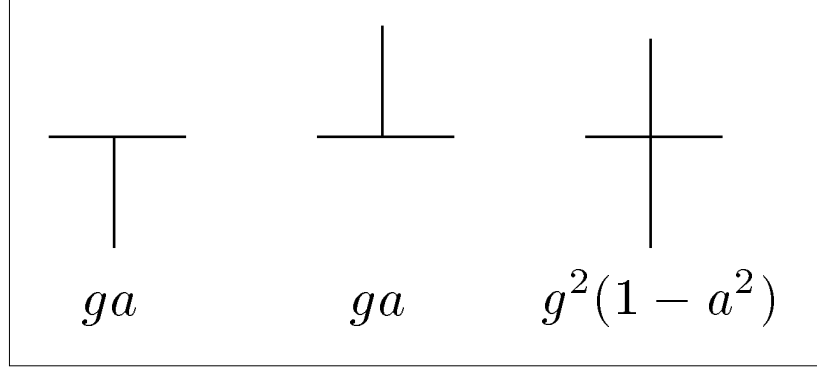


Fig. 3: The Boltzmann weights of the square and triangle formulation of the curvature model for discrete 2D Lorentzian gravity. We have also represented a typical world-sheet configuration in this new interpretation, together with its dual, made of squares and triangles.

is picked, we now have a pair of a lower and an upper half-edge which we can regroup so as to form a crossing of the time line (see Fig.3). Such crossings come with a weight factor $g^2(1 - a^2)$. Finally, the numerator gxy in (2.25) is there to ensure staircase boundary conditions for these new configurations. It corresponds to adding a lower half-edge at the far left and an upper one at the far right, each of which comes with a factor \sqrt{g} only (and no a).

We thus get another representation for the configurations contributing to the transfer matrix element $T_{i,j}(g, a)$, with the Boltzmann weights defined in Fig.3. Dually, these correspond to supplementing the triangulations we have considered so far, by *squares* with two time-like and two space-like edges (see the example of a world-sheet configuration and its dual depicted in Fig.3). All the weights have now been translated into different fugacities for the triangles and for the squares. Each triangle comes with a weight ga , while each square receives a weight $g^2(1 - a^2)$. Note that this latter weight is positive or negative according to whether a is larger or smaller than 1. Finally, the case of the boundary triangles is special since they receive a weight \sqrt{g} only. Let us also mention that,

in the limit $a \rightarrow 0$ corresponding to a regular lattice, only squares and boundary triangles survive, in which case it is clear that the only possible arrangement for the tessellation is regular and the transfer matrix is the identity matrix as it should be.

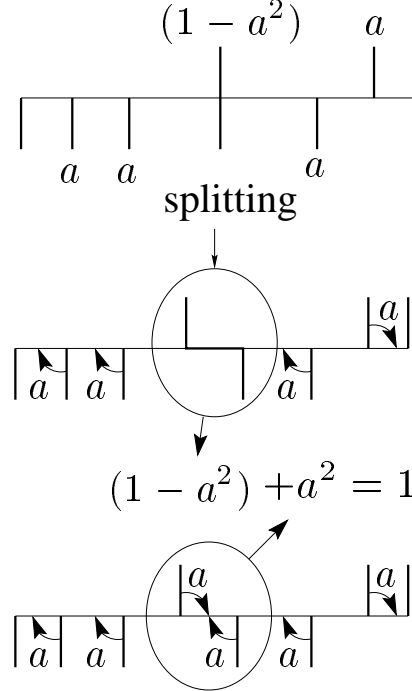


Fig. 4: The connection between square-triangle tessellations and simple triangulations is done by splitting each square (i.e. each crossing) into two triangles (i.e into two half-edges). To recover the proper curvature weight, we transfer the a factors as shown by the arrows. We then add up weights corresponding to the same final triangulation.

To make the contact with the curvature model, the idea is to split each square of the tessellation into a pair of triangles. To recover the proper curvature weights, we chose to split each square into a down triangle followed by an up one. Now the same triangulation is obtained from several square-triangle tessellations and the matrix element $T_{i,j}(g, a)$ is obtained by summing over all these configurations. In the dual language, our splitting corresponds to separating each crossing into a lower and an upper half, such that the upper-half sits at the *left* of the lower one (see Fig.4). As far as the g factors are concerned, since each crossing receives a factor g^2 , which after splitting, gives a weight g per half edge, it is clear that these factors are well taken into account. The \sqrt{g} factors at the boundary are also correct. The a factors are more subtle. Before we collect all these factors, we remark that we can transfer the weight a of each lower half-edge, which

is not at the left boundary, to the horizontal link sitting just above it and to its left (see Fig.4). Similarly, we transfer the factor a attached to each upper half-edge, which is not at the right boundary, to the horizontal link sitting just below to its right. Then all the horizontal links which separate two lower half-edges (resp. two upper half-edges) receive a factor a from their right lower half-edge (resp. their left upper half-edge) as they should in the curvature language, while all the horizontal links with a lower half-edge on the left and an upper half-edge on the right receive a factor 1 as they should. Finally the horizontal links with an upper half-edge on the left and a lower half-edge on the right receive a weight a^2 from the two half-edges, together with a contribution $(1 - a^2)$ coming from the configuration where these two half-edges were connected to form a crossing. Adding these weights restores a factor 1, as required.

2.5. Dimers

From our experience with two-dimensional Euclidean quantum gravity we know that the simplest way of introducing matter in two-dimensional universes is to allow for dimers. Dimers are decorated links which have a certain weight associated with them and each triangle in a triangulation can carry at most one dimer. It is well known that by fine-tuning the weight of the dimers in two-dimensional Euclidean quantum gravity to some specific negative value one can reach a critical point where the universality class of the underlying geometrical system changes from that of pure gravity to that characteristic of gravity coupled to non-unitary matter with central charge $c = -22/5$. It is therefore interesting to note that our model of triangles and squares can be viewed as a simple dimer model. This interpretation simply comes about if one views each square as consisting of two triangles sharing a dimer which lies along either one of the diagonals of the square. In this picture the triangle building blocks do not have any dimers associated with them. The weight of a square, $g^2(1 - a^2)$ is hence to be understood as $2 \cdot (ga)^2((1 - a^2)/(2a^2))$ where ga is the weight of a triangle, $(1 - a^2)/(2a^2)$ is the weight of a dimer and the factor 2 in front takes into account that there are two ways of placing the dimer inside the square. From this decomposition it follows that if new critical behaviour occurs it should happen at a value of a for which $a > 1$. However, it is important to note that our model only includes a subset of configurations of the full dimer model since we do not have any dimers on the space-like links. Thus, if we do not see any new critical behaviour for the model in question it does not necessarily imply that such behaviour does not occur for the full dimer model. In this connection, let us mention that there have been studies of two-dimensional

Euclidean quantum gravity coupled to dimers in a spirit similar to this one. Namely, one has calculated loop-loop correlation functions as a function of distance, not leaving out any matter configurations but modifying the concept of distance so as to avoid dimers on the entrance and exit loop. In that approach a continuum behaviour different from that of pure gravity was seen [11].

2.6. Solution and continuum limit

The property (2.23) yields immediately the generating function of the T -th power of the transfer matrix, describing a world-sheet of time-size T :

$$\begin{aligned}\theta_{q,T}(x,y|\lambda) &= \sum_{i,j \geq 1} x^i y^j Z_{i,j}(T|g,a) \\ &= \sum_{i,j \geq 1} x^i y^j [T_q(\lambda)^T]_{i,j} \\ &= \frac{xy(1-q^2)\lambda^{\frac{T}{2}}}{(1-qx)(1-yy) - \lambda^T(q-x)(q-y)}.\end{aligned}\tag{2.26}$$

for all $T = 0, 1, 2, \dots$

As noted in [13], one can derive a continuum limit of the expression (2.26), that corresponds in our notations to the limit $q \rightarrow 1$ ($ga \rightarrow a/(a+1)$). The critical values $x = y = 1$ (corresponding to the limiting convergence radii of the series $F_m(x|q)$ and $F_m(y|q)$) must be approached simultaneously. We see then from (2.26) that λ must also tend to 1 for the expression to remain finite. But from (2.19), a natural way to realize the latter limit is to simply keep a constant while $q \rightarrow 1$ (and $g \rightarrow 1/(a+1)$).

Let us therefore perform the following scaling transformations for some small parameter α

$$T = \frac{\tau}{\alpha}, \quad x = 1 - \alpha X, \quad y = 1 - \alpha Y, \quad q = e^{-\alpha\sqrt{\Lambda}},\tag{2.27}$$

where Λ is the renormalized cosmological constant, τ the continuous time variable, and α an infinitesimal parameter with the dimension of a length. This corresponds in turn to the scaling behaviour

$$\lambda = 1 - 2a\alpha\sqrt{\Lambda} + \mathcal{O}(\alpha^2), \quad g = \frac{1}{a+1}\left(1 - \frac{a}{2}\alpha^2\Lambda\right) + \mathcal{O}(\alpha^4),\tag{2.28}$$

for *fixed* a . Applying the transformations (2.27) to (2.26), we get the rescaled two-loop generating function

$$\begin{aligned}\Theta(X, Y|\tau, \sqrt{\Lambda}, a) &\equiv \lim_{\alpha \rightarrow 0} \alpha \theta_{q,T}(x, y|\lambda) \\ &= \frac{2\sqrt{\Lambda}e^{-\tau a\sqrt{\Lambda}}}{(X + \sqrt{\Lambda})(Y + \sqrt{\Lambda}) - e^{-2\tau a\sqrt{\Lambda}}(X - \sqrt{\Lambda})(Y - \sqrt{\Lambda})},\end{aligned}\tag{2.29}$$

The actual two-loop correlator

$$G(L_1, L_2|\tau, \sqrt{\Lambda}, a) \equiv \lim_{\alpha \rightarrow 0} \frac{1}{\alpha} Z_{l_1, l_2}(T|g, a), \quad (2.30)$$

with $L_i = \alpha l_i$, $i = 1, 2$ is obtained by performing the inverse Laplace transformation of (2.29), leading to (we have set $\phi = e^{-a\tau\sqrt{\Lambda}}$ for simplicity)

$$\begin{aligned} G(L_1, L_2|\tau, \sqrt{\Lambda}, a) &= \int_{-i\infty}^{i\infty} dX dY e^{L_1 X + L_2 Y} \Theta(X, Y|\tau, \sqrt{\Lambda}, a) \\ &= \int_{-i\infty}^{i\infty} dudv \frac{2\sqrt{\Lambda}\phi e^{\sqrt{\Lambda}(L_1 u + L_2 v)}}{(u+1)(v+1) - \phi^2(u-1)(v-1)} \\ &= 2\sqrt{\Lambda}\phi \int_{-i\infty}^{i\infty} du \frac{e^{\sqrt{\Lambda}\left(L_1 u - L_2 \frac{u(1+\phi^2)+(1-\phi^2)}{u(1-\phi^2)+(1+\phi^2)}\right)}}{u(1-\phi^2) + (1+\phi^2)} \\ &= 2\sqrt{\Lambda}\phi e^{-\sqrt{\Lambda}L_2 \frac{1+\phi^2}{1-\phi^2}} \int_{-i\infty}^{i\infty} du \frac{e^{\sqrt{\Lambda}\left(L_1 u + L_2 \frac{4\phi^2}{1-\phi^2} \frac{1}{u(1-\phi^2)+(1+\phi^2)}\right)}}{u(1-\phi^2) + (1+\phi^2)} \quad (2.31) \\ &= 2\sqrt{\Lambda}\phi e^{-\sqrt{\Lambda}L_2 \frac{1+\phi^2}{1-\phi^2}} \sum_{k \geq 0} \frac{\left(\frac{4\phi^2}{1-\phi^2} \sqrt{\Lambda} L_2\right)^k}{k!} \int_{-i\infty}^{i\infty} \frac{du e^{\sqrt{\Lambda}L_1 u}}{(u(1-\phi^2) + (1+\phi^2))^{k+1}} \\ &= \frac{2\sqrt{\Lambda}\phi}{1-\phi^2} e^{-\sqrt{\Lambda}L_2 \frac{1+\phi^2}{1-\phi^2}} \sum_{k \geq 0} \frac{1}{(k!)^2} \left(\frac{4\phi^2}{(1-\phi^2)^2} \sqrt{\Lambda} L_2\right)^k \frac{d^k}{du^k} e^{\sqrt{\Lambda}L_1 u} \Big|_{u=-\frac{1+\phi^2}{1-\phi^2}} \\ &= \frac{2\sqrt{\Lambda}\phi}{1-\phi^2} e^{-\sqrt{\Lambda}(L_1+L_2) \frac{1+\phi^2}{1-\phi^2}} \sum_{k \geq 0} \frac{1}{(k!)^2} \left(\frac{4\phi^2}{(1-\phi^2)^2} \Lambda L_1 L_2\right)^k, \end{aligned}$$

where we have first made the change of variables $X = u\sqrt{\Lambda}$ and $Y = v\sqrt{\Lambda}$, and then used the Cauchy formula to express the integral as a sum over residues (only one pole in v contributes, located at $v(u) = -(u(1+\phi^2) + (1-\phi^2))/(u(1-\phi^2) + (1+\phi^2))$, whereas only the multiple poles at $u = (1+\phi^2)/(\phi^2-1)$ occur). In terms of the rescaled variables, the two-loop correlator reads finally

$$\begin{aligned} G(L_1, L_2|\tau, \sqrt{\Lambda}, a) &= \frac{\sqrt{\Lambda}}{\sinh(a\tau\sqrt{\Lambda})} e^{-\sqrt{\Lambda}(L_1+L_2)\text{cotanh}(a\tau\sqrt{\Lambda})} I_0\left(\frac{2\sqrt{\Lambda}L_1L_2}{\sinh(a\tau\sqrt{\Lambda})}\right), \quad (2.32) \end{aligned}$$

where I_0 is the modified Bessel function $I_0(x) = \sum_{k \geq 0} (x/2)^{2k}/(k!)^2$.

A few remarks are in order. First note that the dependence on the curvature parameter a is quite simple, and that the physics of the model is not affected by it. So we must draw

the rather negative conclusion that the introduction of curvature in the model cannot change its scaling behaviour. It has just shifted the critical value of g (from $1/2$ for the pure gravity case to $1/(a+1)$ in the model with curvature). Moreover the explicit dependence on a can be entirely absorbed in redefinitions of L_1, L_2, Λ and G , namely $L_1 \rightarrow aL_1$, $L_2 \rightarrow aL_2$, $\Lambda \rightarrow \Lambda/a^2$ and $G \rightarrow aG$. This “triviality” of the curvature dependence will be explained in Sect. 3 below, from a very different perspective.

As a final consistency check, let us compute the $a \rightarrow 0$ limit of the two-loop correlator (2.32). Using the asymptotics of the Bessel function $I_0(x) \sim e^x/\sqrt{2\pi x}$ for large x , we get

$$\begin{aligned}
G(L_1, L_2 | \tau, \sqrt{\Lambda}, a \rightarrow 0) &\sim \frac{e^{-\frac{1}{\tau a}(\sqrt{L_1} - \sqrt{L_2})^2}}{\sqrt{4\pi\tau a\sqrt{L_1 L_2}}} \\
&\rightarrow \frac{1}{2\sqrt{L_1}} \delta(\sqrt{L_1} - \sqrt{L_2}) = \delta(L_1 - L_2),
\end{aligned} \tag{2.33}$$

where we have used the limit $\lim_{s \rightarrow 0^+} e^{-x^2/s}/\sqrt{\pi s} = \delta(x)$. We recover therefore the expected flat world-sheet result (also stated as $Z_{\ell_1, \ell_2}(T|1, 0) = \delta_{\ell_1, \ell_2}$).

2.7. Other Boundary conditions

In [13], where boundary conditions were chosen to be periodic, the result for the two-loop correlator in the scaling limit is very similar to (2.31) except that $a = 1$ (no curvature) and more importantly that the modified Bessel function I_0 is replaced by I_1 . We have a very simple explanation for this fact, that involves computing the p -seam loop correlator which we will define now. Up to now, we only considered triangulations with “staircase” boundary conditions. Let us denote these triangulations as being of type (I). Starting from such a type (I) triangulation in its dual picture, a seemingly easy way to get periodic boundary conditions would be simply to identify the left and right staircase boundaries of the triangulation to construct a cylinder marked by a seam, remnant of the staircase. This construction is however problematic. Indeed, on each horizontal step of the left staircase boundary, we can have an arbitrary number of incoming lower half edges. Similarly, on any horizontal step of the right staircase boundary, we have an arbitrary number of incoming upper half-edges. When connecting these two staircases, there is no well defined natural prescription for deciding how to place these lower and upper half edges with respect to one-another.

To overcome this problem, we need to introduce a new type of triangulations, which we will call type (II), and which can be glued without ambiguity to a type (I) triangulation.

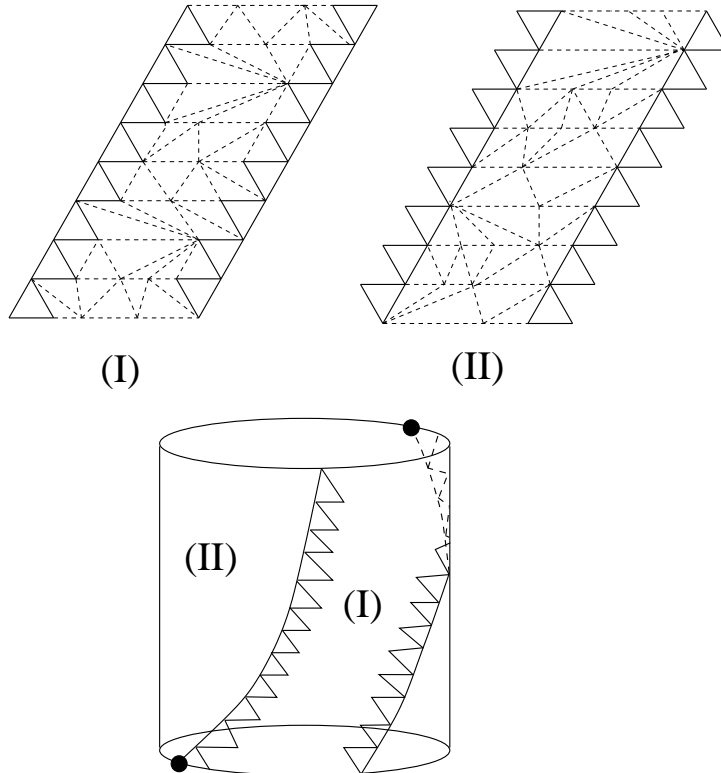


Fig. 5: An example of triangulation of type (I) and a triangulation of type (II). The boundary chaplets serve as seams to connect type (I) to type (II) triangulations. We give an example of cylinder made of two glued triangulations. Any marked point (black dot) on the lower (resp. upper) loop defines a unique chaplet of triangles pointing up (resp. pointing down).

Let us first see how the existence of a “staircase” in the dual representation translates into the original (i.e. non-dual) representation made of triangles. Each leftmost lower half-edge of the dual picture becomes a triangle pointing up. Each such leftmost triangle is attached by its lower left vertex to the upper vertex of the leftmost triangle in the layer just below, so as to form a chaplet (see Fig.5). Similarly, the right staircase translates into a chaplet of triangles pointing down, each triangle being attached by its upper right vertex to the lower vertex of the triangle in the layer just above. The “space” between these two chaplets is filled with strips of triangles of arbitrary length, including strips of length zero corresponding to the case where the two chaplets would be in contact. The two chaplets will serve as seams in our construction. In order to glue our type (I) triangulation to a type (II) triangulation, this type (II) triangulation must itself have boundaries made of chaplets but now with the reverse convention, i.e. with a chaplet of triangles pointing up as its right boundary and a chaplet of triangles pointing down as its left boundary (see

Fig.5). Again, the space between these chaplets is to be filled with strips of arbitrary, possibly zero, length. It is clear that we can glue a type (I) triangulation to a type (II) triangulation on any side by simply superimposing the left (resp. right) chaplet of the former to the right (resp. left) chaplet of the latter. We can thus construct a p -seam loop correlator by gluing p triangulations of alternating type (I) and (II), and, assuming that p is even, gluing the last triangulation to the first one so as to form a cylinder (see Fig.5 for $p = 2$). If the number p of triangulations is odd, we can build an open object with $p - 1$ seams and either type (I) or type (II) boundary conditions, depending on whether to two extremal triangulations are of type (I) or of type (II). This construction gives a nice a posteriori explanation for our choice of weight \sqrt{g} per boundary half-edge: this is because the edges (or the triangles) have to be identified by pairs to form the seam, hence the weight is right to get a factor g per half-edge of the seam.

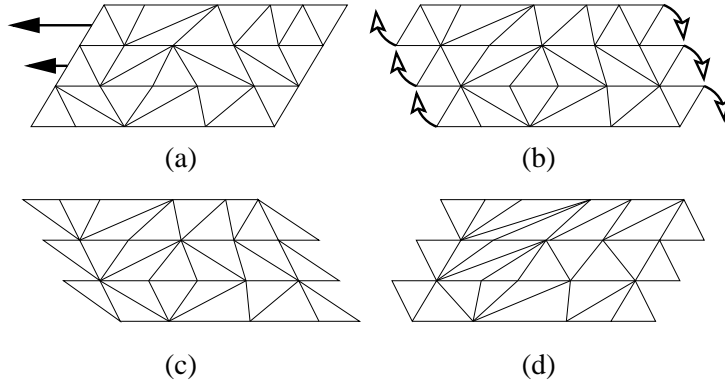


Fig. 6: The one-to-one correspondence between type (I) and type (II) triangulations. Starting from a type (I) triangulation (a), we move each slice one step to the left with respect to the slice just below to obtain (b). We then send the lower left and upper right vertices of the boundary triangles thus released in each slice to respectively upper left and lower right position to obtain the type (II) triangulation (c), or equivalently (d). The passage from (a) to (d) is clearly invertible.

We have computed in Sect. 2.1 the transfer matrix for type (I) triangulations, given by (2.2). A remarkable result is that, although type (II) triangulations are different from type (I) triangulations, the transfer matrix for type (II) triangulations is *identical* to that of type (I), i.e.

$$T_{i,j}^{(II)}(g, a) = T_{i,j}^{(I)}(g, a) = T_{i,j}(g, a), \quad (2.34)$$

with $T_{i,j}(g, a)$ given by (2.2). To understand this property, we remark that starting from a type (I) triangulation, we can deform it into a type (II) triangulation by simply letting

each time slice move one step to the left with respect to the slice just below, and by sending the lower left and upper right vertices of the boundary triangles so released in each slice, to respectively upper left and lower right positions (see Fig.6). This transformation is clearly invertible, hence the announced result (2.34).

Thanks to the above construction, we may define and compute the p -seam two-loop correlator by juxtaposing side by side p copies of alternating (I) and (II) triangulations, with a total lower (resp. upper) loop length of ℓ_1 (resp. ℓ_2), in which we simply have to identify the consecutive chaplet boundaries (again, the boundary weights produce the desired weight g per half-edge of seam). Assuming p even and gluing the last triangulation to the first one, this leads to the p -seam two-loop correlator

$$Z_{\ell_1, \ell_2}^{(p)}(T|g, a) = [(T(g, a) \otimes T(g, a) \otimes \dots \otimes T(g, a))^T]_{\ell_1, \ell_2} \quad (2.35)$$

where there are p factors in the tensor product, and the matrix element (ℓ_1, ℓ_2) actually corresponds to the sum over all p -tuples of pairs of indices (m_i, n_i) for each $T(g, a)$, with $\sum_i (n_i - 1/2) = \ell_1$ and $\sum_i (m_i - 1/2) = \ell_2$. In terms of generating functions, the p -seam correlator (2.35) is simply generated by:

$$\theta_{q, T}^{(p)}(x, y|\lambda) = \left(\frac{\theta_{q, T}(x, y|\lambda)}{\sqrt{xy}} \right)^p, \quad p \text{ even} . \quad (2.36)$$

For odd p , gluing p triangulations of alternating type (I) and (II) leads to an open object of either type (I) or type (II) with the two-loop correlator now generated by:

$$\theta_{q, T}^{(p)}(x, y|\lambda) = \sqrt{xy} \left(\frac{\theta_{q, T}(x, y|\lambda)}{\sqrt{xy}} \right)^p, \quad p \text{ odd} . \quad (2.37)$$

Let us now perform the scaling transformations (2.27) on (2.36) or (2.37). We obtain the p -seam scaling function (note that it has required a multiplication by α^p to produce a finite limit)

$$\Theta^{(p)}(X, Y|\tau, \sqrt{\Lambda}, a) = \Theta(X, Y|\tau, \sqrt{\Lambda}, a)^p. \quad (2.38)$$

We get the corresponding two-loop correlator by applying the inverse Laplace transform,

and performing integrations analogous to those of (2.31):

$$\begin{aligned}
G^{(p)}(L_1, L_2 | \tau, \Lambda, a) &= \int_{-i\infty}^{i\infty} dX dY e^{L_1 X + L_2 Y} \Theta(X, Y | \tau, \sqrt{\Lambda}, a)^p \\
&= \Lambda \int_{-i\infty}^{i\infty} dudve^{\sqrt{\Lambda}(L_1 u + L_2 v)} \left(\frac{2\phi}{\sqrt{\Lambda}((u+1)(v+1) - \phi^2(u-1)(v-1))} \right)^p \\
&= \int_{-i\infty}^{i\infty} \frac{du}{(p-1)!} \frac{(2\phi)^p \Lambda e^{\sqrt{\Lambda} L_1 u}}{(\sqrt{\Lambda}(u(1-\phi^2) + (1+\phi^2)))^p} \frac{d^{p-1}}{dv^{p-1}} e^{\sqrt{\Lambda} L_2 v} \Big|_{v=-\frac{u(1+\phi^2)+(1-\phi^2)}{u(1-\phi^2)+(1+\phi^2)}} \\
&= \frac{\sqrt{\Lambda}(2\phi L_2)^p}{(p-1)! L_2} \int_{-i\infty}^{i\infty} du \frac{e^{\sqrt{\Lambda} \left(L_1 u - L_2 \frac{u(1+\phi^2)+(1-\phi^2)}{u(1-\phi^2)+(1+\phi^2)} \right)}}{(u(1-\phi^2) + (1+\phi^2))^p} \\
&= \frac{\sqrt{\Lambda}(2\phi L_2)^p}{(p-1)! L_2} \sum_{k \geq 0} \frac{1}{k!} \left(\frac{4\phi^2}{1-\phi^2} \sqrt{\Lambda} L_2 \right)^k \int_{-i\infty}^{i\infty} du \frac{e^{\sqrt{\Lambda} \left(L_1 u - L_2 \frac{1+\phi^2}{1-\phi^2} \right)}}{(u(1-\phi^2) + (1+\phi^2))^{p+k}} \\
&= \frac{2\phi \sqrt{\Lambda} (\sqrt{L_1 L_2})^{p-1}}{(1-\phi^2)(p-1)!} e^{-\sqrt{\Lambda}(L_1+L_2) \frac{1+\phi^2}{1-\phi^2}} \sum_{k \geq 0} \frac{\left(\frac{2\phi}{1-\phi^2} \sqrt{\Lambda L_1 L_2} \right)^{2k+p-1}}{k!(k+p-1)!},
\end{aligned} \tag{2.39}$$

for $p \geq 1$. In terms of the rescaled variables, the p -seam two-loop correlator reads

$$\begin{aligned}
G^{(p)}(L_1, L_2 | \tau, \Lambda, a) &= \frac{\sqrt{\Lambda} (\sqrt{L_1 L_2})^{p-1}}{\sinh(a\tau \sqrt{\Lambda})(p-1)!} e^{-\sqrt{\Lambda}(L_1+L_2) \coth \operatorname{arctanh}(a\tau \sqrt{\Lambda})} I_{p-1} \left(\frac{2\sqrt{\Lambda L_1 L_2}}{\sinh(a\tau \sqrt{\Lambda})} \right),
\end{aligned} \tag{2.40}$$

where I_m denotes the m -th modified Bessel function, defined by the series $I_m(x) = \sum_{k \geq 0} (x/2)^{m+2k} / (k!(m+k)!)$.

When $p = 1$ this reduces to (2.32), as it should. More interestingly, when $p = 2$, in the pure gravity case $a = 1$, the expression reduces, up to a factor of L_2 , to the result for the two-loop correlator in periodic boundary conditions with one marked point on the lower loop [12], i.e. equivalently, the two-loop correlator in periodic boundary conditions with one marked point on the lower loop and one marked point on the upper loop (note that marking a point on the external loops simply amounts to multiplying by the length of this loop in the correlator).

One can easily explain this coincidence by noticing that, starting from a cylindrical world-sheet with a marked point, say, on the lower loop, this marked point defines a unique chaplet of up triangles crossing the cylinder from the lower to the upper loop. Indeed this point is the lower left vertex of a unique up triangle in the first slice, whose upper vertex

is itself the lower left vertex of a unique triangle in the second slice, and so on (see Fig.5). Similarly, any marked point on the upper loop defines a unique chaplet of triangles pointing down. Thus marking a point on the upper loop and one on the lower loop amounts to marking two chaplets, one made of up triangles and one made of down triangles. Such chaplets cannot intersect and thus divide the cylinder into two triangulations, one of type (I) and one of type (II). This explains the connection between the two-seam two-loop correlator and the periodic loop correlator. Note that this nice property breaks down as soon as $p > 2$ because, for more than one point on each external loop, we cannot guaranty for arbitrary chosen marked points that the corresponding chaplets alternate along the cylinder between “up” and “down” chaplets, which is crucial to keep our interpretation as p -seam correlator. In particular two successive chaplets of the same (up or down) type can now merge into a single chaplet.

Note finally that we have the following relation between our $(2p + 2)$ -seam correlator and the amplitude A_p (with $p + 1$ a type of winding number) obtained by Nakayama in a continuum calculation using proper time gauge [14]

$$G^{(2p+2)}(L_1, L_2 | \tau, \Lambda, a = 1) = \frac{(L_1 L_2)^p \sqrt{L_1 L_2}}{(2p + 1)!} A_p. \quad (2.41)$$

3. Lorentzian Triangulations as Random Walks

In this section, we will discuss the equivalence between Lorentzian gravity configurations and ordinary random walk (RW) configurations in one dimension. This connection will allow us to re-phrase the quantities computed above in the language of RW statistics. For instance we will see how the two-loop correlator of Lorentzian gravity relates to a well-known generating function for the large excursions of a Brownian motion. This equivalence will also explain why Lorentzian triangulations have fractal dimension 2 and why introducing a curvature weight (i.e. taking $a \neq 1$) cannot change the continuum large scale properties of Lorentzian gravity, as found in Sect. 2.4. Finally, the RW picture will also provide a very direct derivation of the crucial property (2.23) for the product of two transfer matrices.

3.1. Equivalence between Lorentzian triangulations and random walks

The random triangulations describing Lorentzian gravity can be seen as deformations of a regular triangular lattice. More precisely, if we view the regular triangular lattice as made of regular time slices of *alternating* up and down triangles, then removing some of these triangles and gluing together the remaining ones along their time-like edges within each strip leads to a triangulation like that of Fig.1. Conversely, we can, starting from a random triangulation of this type, insert a number of additional triangles to make it regular. It is therefore possible to visualize a random triangulation as a regular one with two types of triangles: “real” triangles which are to be kept and form the triangulation and “virtual” triangles which have to be shrunk or removed.

This splitting procedure into real and virtual triangles can be made according to a well defined procedure which we shall now describe, and which takes the form of a one-to-one correspondence between Lorentzian triangulations and directed random walks drawn on the regular triangular lattice.

The equivalence is as follows:

Consider a directed random walk drawn on the regular lattice, starting at “height” $h = 0$, making $\Delta h = \pm 1$ steps to the right and ending at height $h = T + 1$ after S steps (see Fig.7). Since the walk is directed, the horizontal direction can be viewed as well as an effective time dimension for the random walk whose motion takes place in the one dimensional vertical h -direction. This height variable h will however correspond to the time variable t of the triangulation, with each time slice t lying between heights $h = t - 1$ and $h = t$. The random walk is moreover required to stay confined within the strip $0 \leq h \leq T + 1$. Now to each elementary *ascending* step of the RW between heights h and $h + 1$, we associate the *pair of triangles* of the regular lattice made of the up triangle lying immediately to its right in the time slice $h + 1$ and the down triangle lying just below in the slice h (see Fig.7). These triangles will be the “real” triangles to be kept in the triangulation. Removing all the other triangles and gluing the real ones together along their time-like edges, we end up with a random Lorentzian triangulation of width T , and decorated by l_1 down triangles in time slice $t = 0$ and l_2 up triangles in time slice $t = T + 1$. These extremal time slices are then removed to recover the relevant triangulation. Note that from the above construction where we add triangles only to the right of the ascending

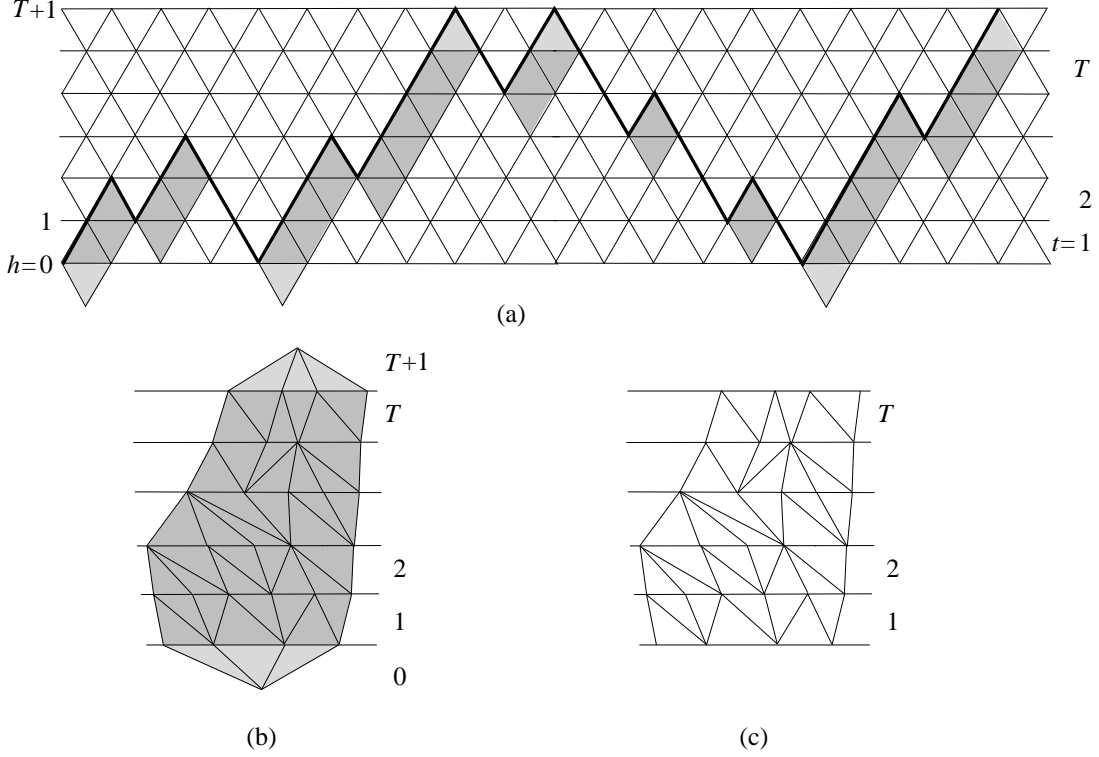


Fig. 7: Starting from a directed random walk (a) drawn on the regular triangular lattice, we associate to each ascending step of the walk the pair of triangles lying just below it (grey triangles). We then eliminate all the other triangles and glue the grey triangles together along their time-like edges inside each strip, thus forming a random Lorentzian triangulation (b). The 0 and $T + 1$ slices (light-grey triangles) are finally removed (c).

steps, it follows that the resulting triangulation satisfies the staircase condition of Sect. 2.1⁷.

We can thus associate to each directed RW of the type described above a Lorentzian triangulation with staircase boundary conditions. Let us now describe how, starting now from such a Lorentzian triangulation, we recover the associated RW. This reverse construction can be performed in three steps as shown in Fig.8. The first step is to go to the dual representation of the triangulation (Fig.8-b). In a second step, the dual world-sheet configuration can be transformed into a tree configuration (Fig.8-c) by attaching each vertical dual bond to the bond sitting in the strip just below and to its left. In a third step, this tree-like structure is transformed into a directed random walk (Fig.8-d) by simply following

⁷ Note that the triangles can be viewed as well as being added on the left side of the descending slopes of a directed walk, now going from height $h = T$ and reaching height $h = -1$ after S steps to the left.

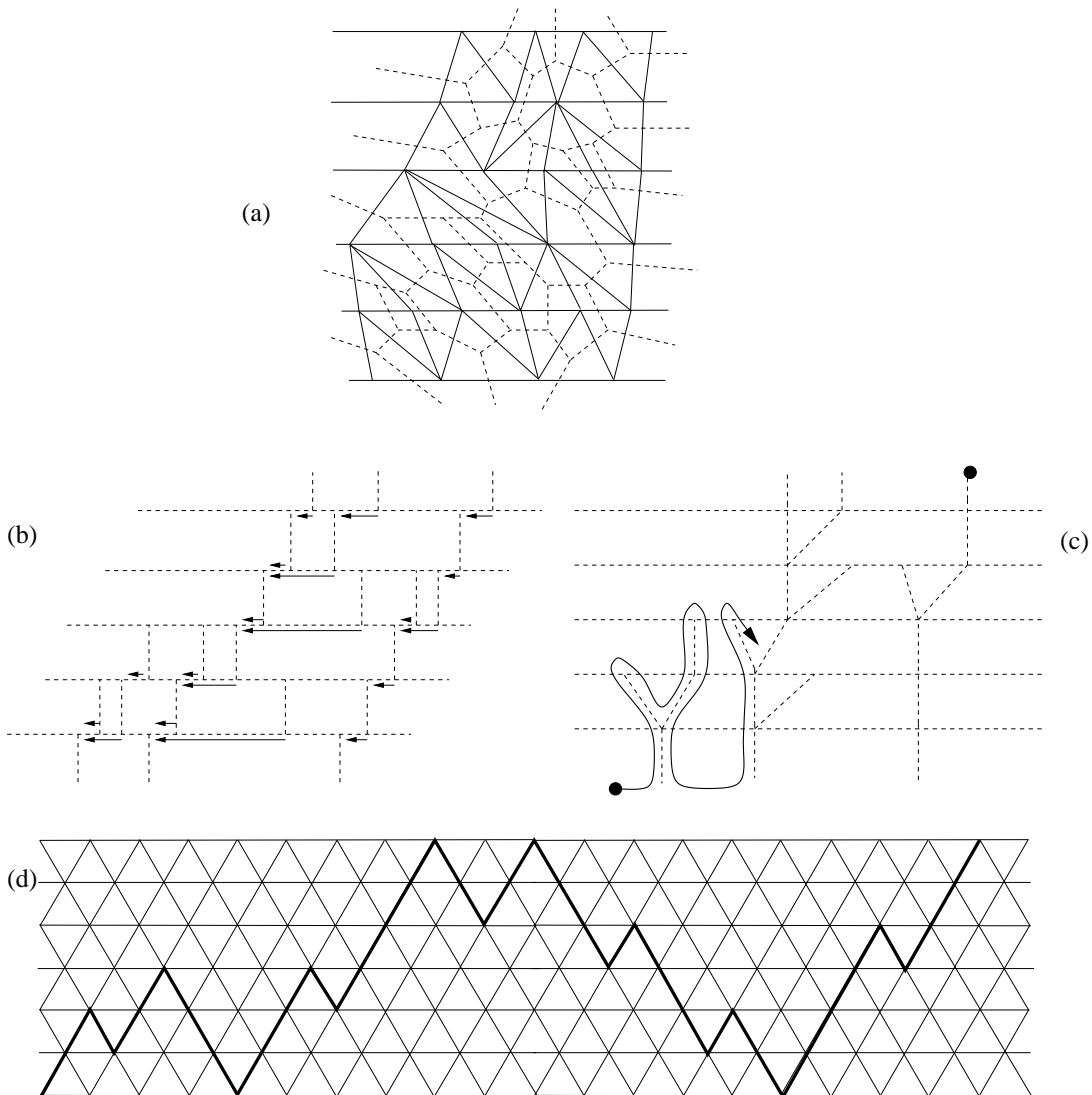


Fig. 8: Starting from a Lorentzian triangulation satisfying staircase boundary conditions (a), we go to the dual configuration (b) and attach each vertical dual bond to the bond to its left in the preceding strip, as shown by the arrows, to get a tree structure (c). Following the contour of the trees from the lower left branch to the upper right one (black points), the sequence of ascents and descents can be translated into a directed random walk (d).

the contour of the trees from the lower left branch to the upper right one and making a step $\Delta h = +1$ for each ascent along a branch and a step $\Delta h = -1$ for each descent along a branch. It is easy to check that the resulting RW is precisely the expected one.

Our main result here is thus a *one-to-one correspondence* between directed random walks and Lorentzian triangulations, which in turn implies a direct equivalence for the various quantities describing them. Some of these relations will be described in the next

section. Let us simply note here that we can deal with all types of boundary conditions. The staircase boundary condition described in this section corresponds to random walks starting at $h = 0$ and ending at height $h = T + 1$. The case of walks starting and ending at $h = 0$ would describe periodic boundary conditions with a marked point in the lower loop of the triangulation.

3.2. Two-loop correlator as a generating function for large excursions

Let us now re-interpret some of the natural statistical properties of random Lorentzian triangulations in the language of random walks.

Since we associate a pair of triangles to each ascending step, the number N_t of triangles is directly related to the length S of the walk by:

$$N_t + (l_1 + l_2) = S + T + 1. \quad (3.1)$$

Here N_t counts all the triangles with $1 \leq t \leq T$, ignoring the $(l_1 + l_2)$ triangles in the slices $t = 0$ and $t = T + 1$ which are removed in the construction of the triangulation. We also used the fact that there are $T + 1$ more ascending steps than descending steps in the walk. Setting $a = 1$ for the time-being, the triangulation comes with a factor $g^{N_t - T}$ due to the particular treatment of the extremal left and right triangles in each of the T slices. The corresponding weight $g^{S - (l_1 + l_2 - 1)}$ can be interpreted as a fugacity g *per step* for the random walk, together with a reflection factor $(1/g)$ for each of the l_1 contacts at $h = 0$ or the l_2 contacts at $h = T + 1$, except for the last contact. Note that for the critical value $g = 1/2$, we can view these weights as a probability $1/2$ for the walk to make a step up or down inside the strip and a probability 1 for the walk to make an up (resp. a down) step at the $h = 0$ (resp. $h = T + 1$) boundary, i.e. we have an unbiased random walk between two reflecting walls.

The sizes l_1 and l_2 of the bottom and top loops of the triangulation correspond precisely to the number of contacts at $h = 0$ and at $h = T + 1$ respectively. We can thus reinterpret the two-loop correlator $Z_{l_1, l_2}(T|g, a = 1)$ as the generating function

$$Z_{l_1, l_2}(T|g, a = 1) = \frac{1}{(2g)^{l_1 + l_2 - 1}} \sum_{S \geq 0} (2g)^S P_T(l_1, l_2, S) \quad (3.2)$$

where $P_T(l_1, l_2, S)$ is the probability for an unbiased walker starting at $h = 0$ and evolving between two reflecting walls at $h = 0$ and $h = T + 1$ to reach the wall $h = T + 1$ in S steps

after exactly l_1 contacts (including the first one) at the bottom wall and l_2 (including the last one) at the top wall.

More generally, if we re-instate the factor x (resp. y) per space like link in the bottom (resp. top) loop, the triangulation generating function $\theta_T(x, y|g, a = 1)$ (given by Eq. (2.26) for $a = 1$, i.e. $q = (1 - \sqrt{1 - 4g^2})/(2g)$ and $\lambda = q^2$) becomes the generating function for random walks between two walls with a weight g per step and a weight x/g (resp. y/g) per contact to the bottom (resp. the top) wall. In the RW language, we call each portion of walk between two *successive* contacts an “excursion”. Since the walk is a Markov process, each of these excursions is an independent random object. Excursions here are of four types: bottom-bottom and top-top excursions, which have the same generating function (up to the exchange of x and y), and bottom-top and top-bottom excursions which also have the same generating function. For instance the bottom-bottom excursion counts the walks starting and ending at $h = 0$ and *staying below* $h = T$. The distribution probability for, say, the height and the length of bottom-bottom excursions is a basic quantity of the random walk statistics and enters many different physical problems. Its continuous, Brownian motion limiting scaling expression is well known, as are many other more involved excursion properties appearing in many different areas of physics. As an example, we would like to show here how the two-loop correlator of Lorentzian gravity directly relates to a well known probability distribution describing the diffusion of a particle in a one-dimensional random energy landscape.

The diffusion of a particle in a random energy landscape can be modelled by the so-called Sinai model [20], where a particle jumps to one of its two neighbouring sites with a probability $p \propto \exp(-\Delta U)$ involving the energy difference ΔU with this neighbouring site. If we represent the energy landscape as a random walk, with the height $h \propto U$ corresponding to the energy, a bottom-bottom excursion describes an energy barrier of height less than T . Exact expressions for the large time properties of the diffusion have been obtained and it was recognized that a good way to recover these expressions is to assume that the particle at time t is *localized* precisely in the lowest energy minimum it can reach by passing all the energy barriers of height less than a certain maximal size $T(t)$, with the relation $T(t) \propto \ln(t)$. Let us for instance consider the example of Fig.9 (b) where a particle, starting at a wall, jumps to the right by passing all barriers of height strictly less than T , looking for lower and lower minima to the right until it reaches a barrier of

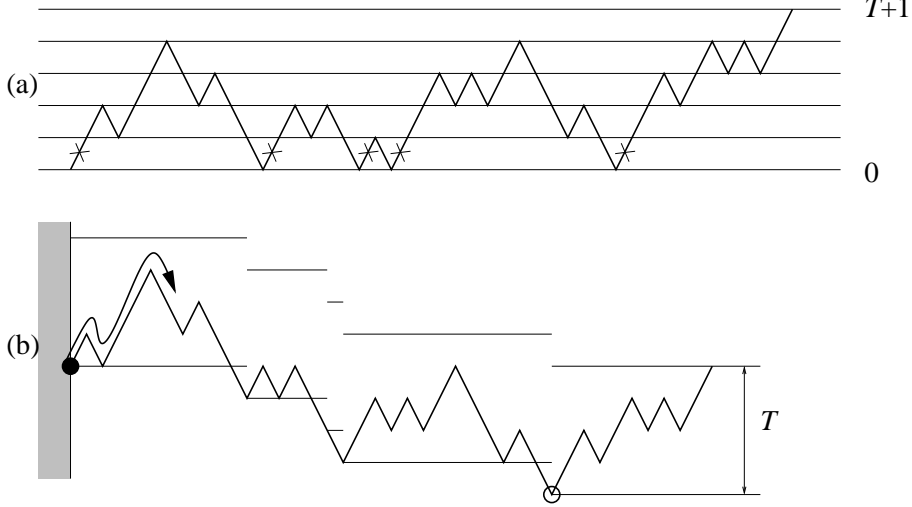


Fig. 9: (a) A random walk entering the definition of $Z_{m+1,1}(T|g, a)$, i.e. with $m + 1$ contacts (here $m = 4$) at $h = 0$ and 1 contact at $h = T + 1$. (b) The corresponding energy landscape obtained by erasing in (a) all the ascending steps following immediately a contact at $h = 0$. The deepest minimum reachable by a diffusing particle (black dot) passing energy barriers of height strictly less than T is at depth m (white circle).

height larger than or equal to T . How far and how deep does the particle go? From (3.2), we know that the quantity

$$Z_{l_1=m+1, l_2=1}(T|g, a = 1) = \frac{1}{(2g)^{m+1}} \sum_{S \geq 0} (2g)^S P_T(m + 1, 1, S), \quad (3.3)$$

relates to the probability $P_T(m + 1, 1, S)$ that the walk reaches $h = T + 1$ for the first time after S steps and passes m times at $h = 0$. If we deform the walk by suppressing the first ascending step after each contact point at $h = 0$, the quantity $P_T(m + 1, 1, S)$ becomes the probability for the diffusing particle to have reached a depth m by passing barriers of length strictly less than T and being blocked after $S - m - 1$ steps by a barrier of height larger or equal to T . Going to the continuous limit and using (2.32), we obtain that the two-loop correlator

$$G(L, 0|\tau = 1, \sqrt{\Lambda}, a = 1) = \frac{\sqrt{\Lambda}}{\sinh(\sqrt{\Lambda})} e^{-\sqrt{\Lambda} L \coth \tanh(\sqrt{\Lambda})}, \quad (3.4)$$

should be equal to the Laplace transform

$$\hat{P}(L, \Lambda) \equiv \int_0^\infty dx P(L, x) e^{-\Lambda x}, \quad (3.5)$$

of the probability density $P(L, x)$ for the particle to reach the deepest minimum at depth L and being blocked at a distance x from the wall, in the scaling limit of large T , m , and S with $m/T = L$ and $S/T^2 = x$ fixed⁸. This probability is the convolution of the probability $P_1(L, x_1)$ that the particle reaches the deepest minimum at depth L and distance x_1 from the wall, and the probability $P_2(x_2)$ that the last excursion to the blocking point is of length x_2 . The expression (3.4) is then a direct consequence of the following expressions

$$\begin{aligned} \hat{P}_1(L, \Lambda) &\equiv \int_0^\infty dx_1 P_1(L, x_1) e^{-\Lambda x_1} = e^{-\sqrt{\Lambda} L \cot \tanh(\sqrt{\Lambda})}, \\ \hat{P}_2(\Lambda) &\equiv \int_0^\infty dx_2 P_2(x_2) e^{-\Lambda x_2} = \frac{\sqrt{\Lambda}}{\sinh(\sqrt{\Lambda})} \end{aligned}, \quad (3.6)$$

which are well known in the context of the Sinai model [21].

The RW equivalence also provides an explanation for the fractal dimension 2 of Lorentzian triangulations. It is well-known that the Brownian motion has fractal dimension 2, meaning that the time (represented here by the length S of the walk) needed to travel over a distance T (here the height $h \sim T$) scales as T^2 . Since S corresponds in our equivalence to the number N_t of triangles, i.e to the area A of the triangulation, we obtain that $A \sim T^2$ and thus get a fractal dimension 2 for Lorentzian triangulations. Note that the fact that l_1 (or l_2) scales as T is also clear in the Sinai model language (with $l_1 \sim m$) where it means that the depth reached by passing maximal barriers of order T is itself of order T .

3.3. Curvature and universality

Let us now re-instate a curvature weight $a \neq 1$ in the problem, and let us see how it translates into the random walk language. As for the equivalence with tessellations of triangles and squares of Sect. 2.4, we can regroup the up and down triangles in each strip as follows. One first re-groups all pairs of triangles made of an up triangle immediately followed to its right by a down triangle and assign a weight g^2 to these pairs. The remaining up triangles necessarily have an up triangle to their right. We thus assign them a weight ga accounting for the fugacity g per triangle and the curvature weight a for their interaction with their right neighbour. Similarly, each remaining down triangle necessarily has a down triangle to its left and again receives a weight ga for the same reasons. With this

⁸ Strictly speaking, the particle is blocked after $S - m - 1$ steps, not S , but this correction scales less rapidly than T^2 and is thus negligible.

construction, all the weights have been collected properly and we simply need an extra factor $1/g$ to correct for the special boundary weights. Otherwise stated, we can assign a weight ga for each triangle and correct with a factor $1/a^2$ for each pair made of an up triangle followed by a down one and a global $1/g$ factor. This way of correcting is alternative to that of Sect. 2.4 consisting in adding squares in the game. Denoting by P the total number of up-down pairs in the whole triangulation, we get a weight:

$$\frac{1}{g^T} \frac{(ga)^{N_t}}{(a^2)^P} . \quad (3.7)$$

Now in the RW picture, it is easy to see that up triangles lie immediately to the right of an ascending step, and that they are followed by a down triangle if and only if the next step is also ascending. In other words, pairs of up-down triangles correspond exactly to pairs made of two successive ascending steps. Denoting by n_{++} (resp. n_{+-} , n_{-+} , n_{--}) the pairs of successive ascending-ascending (resp. ascending-descending, descending-ascending, descending-descending) steps, we have the relations

$$\begin{aligned} n_{+-} &= n_{-+}, \\ P &= n_{++}, \\ T &= n_{++} - n_{--}, \\ S &= n_{++} + n_{+-} + n_{-+} + n_{--} . \end{aligned} \quad (3.8)$$

The first relation simply states that there are as many summits as valleys in the RW landscape. Thanks to these relations and to Eq. (3.1), we can rewrite (3.7) as

$$\frac{g^{S-(l_1+l_2-1)} a^{n_{++}+n_{+-}+n_{-+}+n_{--}+T-(l_1+l_2-1)}}{a^{n_{++}+n_{--}+T}} = g^S \frac{1}{(ga)^{l_1+l_2-1}} a^{n_{+-}+n_{-+}} . \quad (3.9)$$

The introduction of $a \neq 1$ has thus two effects in the RW weight: (i) it changes the interaction of contact with the walls from $(1/g)$ to $(1/ga)$ and (ii) introduces a factor a for each *change of slope* in the walk. Note that the two effects cancel exactly at the walls so that the net contribution is simply a factor a for each change of slope *inside* the strip. Such a weight is nothing but an *extrinsic* curvature energy $E \propto -\ln(a)$ for the one dimensional random walk. It is thus remarkable that the *intrinsic* curvature weight of two-dimensional Lorentzian gravity translates into an *extrinsic* one-dimensional curvature weight for the equivalent random walk problem. Note that according to whether a is less or larger than

one, one has a positive (favoring straight lines) or negative (favoring U-turns) curvature elastic constant.

It is well known that extrinsic curvature is an irrelevant perturbation for the large scale properties of the random walk. At most it introduces a finite correlation length below which the random walk is rigid (positive curvature) or crumpled (negative curvature) but at scales larger than this correlation length, the curvature plays no role. Up to an appropriate rescaling, one thus recovers asymptotically the same continuum limit as without curvature energy. This is precisely what we observed in (2.32).

3.4. Product of two transfer matrices

From the RW picture of Lorentzian triangulations, we can easily re-derive the relation (2.23) for the product of two transfer matrices. Indeed, a two-matrix product element like $[T(g, a)T(g', a')]_{i, j}$ corresponds to a sum with appropriate weights over all Lorentzian triangulations made of exactly *two* time slices, with a fixed number i of up triangles in their lower slice, a fixed number j of down triangles in their upper slice, and with staircase boundary conditions. In the RW representation, we thus have to consider all the random walks in a strip of height three $0 \leq h \leq 3$, starting at $h = 0$, ending at $h = 3$ and having exactly i contacts at $h = 0$ and j contacts at $h = 3$. We thus have to sum over all these RW with a fixed number of contacts at the top and at the bottom of the strip $0 \leq h \leq 3$.

Now we can decompose any such random walk into $i + j - 1$ “blocks” corresponding to the $i + j - 1$ portions of the walk between two successive contacts (see Fig.10). The blocks are of four types, numbered (1) to (4), according to whether these contacts are at the bottom or the top of the strip, namely (see Fig.10): (1) bottom-bottom, (2) top-top, (3) bottom-top, and (4) top-bottom. These blocks differ only by the (up or down) nature of their first and last steps while the intermediate steps form a saw-tooth sequence $\Delta h = \sigma, -\sigma, \sigma, -\sigma, \sigma, -\sigma, \dots$, with $\sigma = 1$ or -1 , of arbitrary (possibly zero) length k . The desired sum over the random walks can be achieved by first choosing one of the $\binom{i+j-2}{i-1}$ allowed sequences for the bottom and top contacts, then summing over all the random walks having this particular sequence of contacts, and finally summing over all sequences. Alternatively, we can attach directly a global weight individually to each of the four block types by summing over all possible intermediate configurations, i.e. over all values of the lengths k .

If we are interested in the matrix-product $T(g, a)T(g', a')$, we must attach a weight ga to each ascending step in the slice $0 \leq h \leq 1$, a weight $g'a'$ to each ascending step in

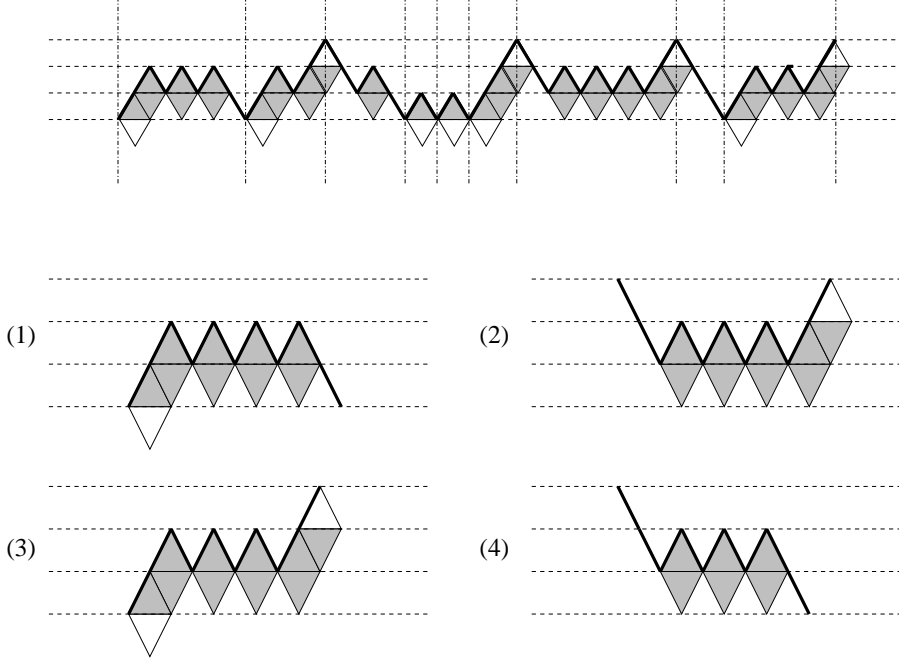


Fig. 10: The decomposition of a walk of height $T + 1 = 3$ into blocks. Each block is a portion of the walk between two successive contacts at the walls $h = 0$ or $h = 3$. The blocs are of four types according to the four possibilities (1) bottom-bottom, (2) top-top, (3) bottom-top and (4) top-bottom for the two contacts at their extremities.

the slice $2 \leq h \leq 3$ and a weight $(gg'aa')$ to each ascending step in the slice $1 \leq h \leq 2$. We then must correct this weight by a curvature factor $1/a^2$ for each sequence $h = 0, 1, 2$ and a factor $1/a'^2$ for each sequence $h = 1, 2, 3$. Gathering these factors and summing over k , we obtain the block weights:

$$\begin{aligned}
 w_2^{(1)} &= ga + \frac{ga}{a^2} \sum_{k=1}^{\infty} (gg'aa')^k = \frac{ga + g^2(1-a^2)g'a'}{1 - gg'aa'}, \\
 w_2^{(2)} &= g'a' + \frac{g'a'}{a'^2} \sum_{k=1}^{\infty} (gg'aa')^k = \frac{g'a' + g'^2(1-a'^2)ga}{1 - gg'aa'}, \\
 w_2^{(3)} &= \frac{(ga)(g'a')}{a^2a'^2} \sum_{k=1}^{\infty} (gg'aa')^k = \frac{g^2g'^2}{1 - gg'aa'}, \\
 w_2^{(4)} &= \sum_{k=0}^{\infty} (gg'aa')^k = \frac{1}{1 - gg'aa'}.
 \end{aligned} \tag{3.10}$$

Note that *all* the weights have been gathered *inside* the blocks and that consecutive blocks do not interact. In order to have the commutation $T(g, a)T(g', a') = T(g', a')T(g, a)$, it is sufficient that the four weights above are invariant under the change $(g, a) \leftrightarrow (g', a')$. This

is readily the case for the weights $w_2^{(3)}$ and $w_2^{(4)}$, while $w_2^{(1)}$ and $w_2^{(2)}$ are exchanged. The commutation condition reads therefore:

$$w_2^{(1)} = w_2^{(2)} \leftrightarrow \frac{1 - g^2(1 - a^2)}{ga} = \frac{1 - g'^2(1 - a'^2)}{g'a'} \equiv q + \frac{1}{q}, \quad (3.11)$$

defining for the two couples (g, a) and (g', a') a common value of q as in (2.5).

To go further and show (2.23), we must compare the product $T(g, a)T(g', a')$ to a single matrix say $T(g'', a'')$. Let us note that the same block decomposition as before can be achieved for random walks in a strip of height two, describing one-slice triangulations contributing to the elements of a single matrix $T(g'', a'')$. In this case, the contact sequence fully specifies the random walk and the four block types correspond to the four possible two step sequences: (1) $\Delta h = +1, -1$, (2) $\Delta h = -1, +1$, (3) $\Delta h = +1, +1$ and (4) $\Delta h = -1, -1$. This leads immediately to the following block weights:

$$\begin{aligned} w_1^{(1)} &= w_1^{(2)} = g''a'', \\ w_1^{(3)} &= g''^2, \\ w_1^{(4)} &= 1. \end{aligned} \quad (3.12)$$

Let us now consider the *same* sequence of blocks with $n^{(i)}$ blocks of type (i) , in both the product $T(g, a)T(g', a')$ and $T(g'', a'')$. On one hand, the weight contribution to $T(g, a)T(g', a')$ is:

$$\frac{1}{gg'} \left(w_2^{(1)}\right)^{n^{(1)}} \left(w_2^{(2)}\right)^{n^{(2)}} \left(w_2^{(3)}\right)^{n^{(3)}} \left(w_2^{(4)}\right)^{n^{(4)}}, \quad (3.13)$$

where the pre-factor $1/gg'$ comes from the special weight of the boundary triangles. On the other hand, the contribution to $T(g'', a'')$ is simply:

$$\frac{1}{g''} \left(w_1^{(1)}\right)^{n^{(1)}+n^{(2)}} \left(w_1^{(3)}\right)^{n^{(3)}}. \quad (3.14)$$

Using the commutation relation (3.11) and the fact that $n^{(3)} = n^{(4)} + 1$, i.e. the number of ‘‘ascending’’ blocks is one unit more than the number of ‘‘descending’’ blocks for the random walks that we consider, we can rewrite (3.13) as:

$$\frac{1}{gg'w_2^{(4)}} \left(w_2^{(1)}\right)^{n^{(1)}+n^{(2)}} \left(w_2^{(3)}w_2^{(4)}\right)^{n^{(3)}}. \quad (3.15)$$

We get therefore obtain the product relation:

$$T(g, a)T(g', a') = \frac{g''}{gg'w_2^{(4)}}T(g'', a''), \quad (3.16)$$

provided that (i) the commutation relation (3.11) is satisfied and (ii) we have the relation:

$$\begin{aligned} w_2^{(1)} = w_1^{(1)} & \leftrightarrow & g'' = \frac{gg'}{1 - gg'aa'} \\ w_2^{(3)}w_2^{(4)} = w_1^{(3)} & & a'' = \frac{ga + g'a' - gg'aa'}{gg'} \left(q + \frac{1}{q} \right) \end{aligned} \quad (3.17)$$

with q as in (3.11) above. It is straightforward to check that the above values of g'' and a'' obey the relation:

$$\frac{1 - g''^2(1 - a''^2)}{g''a''} = q + \frac{1}{q}, \quad (3.18)$$

and thus the three couples $(g, a), (g', a')$ and (g'', a'') correspond to the same value of q . If we introduce the parameter λ as in (2.19) for (g, a) and λ' for (g', a') , the value of λ'' for (g'', a'') is found to be $\lambda'' = \lambda\lambda'$, while the pre-factor in (3.16) disappears since $g''/gg'w_2^{(4)} = 1$. We have therefore proven the relation (2.23) in the language of random walks. One should note that the power of this method comes from the fact that we used only four basic objects, the four blocks, each of which corresponds to a particularly simple family of walks, while the arbitrary sequence of the blocks plays no role. We expect that we can take advantage of such a block decomposition to obtain commutation relations for the transfer matrices of more involved problems of Lorentzian gravity, in particular including matter degrees of freedom.

4. Other Models

4.1. General construction: symmetric case

Let us reconsider the expression (2.18) for the curvature transfer matrix $T_q(\lambda)$ in terms of the generating functions F_m of its eigenvectors. If we now start from some arbitrary orthonormal family $v^{(m)}$, $m = 1, 2, \dots$ of vectors generating some space E , and a given non-zero function $f(\lambda)$, we may easily construct a commuting set of symmetric transfer matrices $T(\lambda)$ with entries

$$T_{i,j}(\lambda) = f(\lambda) \sum_{m \geq 1} v_i^{(m)} \lambda^{m-1} v_j^{(m)}, \quad (4.1)$$

that satisfy the multiplicativity property

$$T(\lambda)T(\lambda') = \frac{f(\lambda)f(\lambda')}{f(\lambda\lambda')}T(\lambda\lambda'). \quad (4.2)$$

We also remark that, given any set of orthonormal vectors, generated say by $F_m(x)$, then the other set generated by $G_m(x) = F_m(x)\varphi(x)$ is also orthonormal, provided we take

$$\varphi(x) = \prod_{j=1}^k \varphi(x|q_j)^{k_j} \quad , \quad \varphi(x|q) = \frac{q-x}{1-qx}, \quad (4.3)$$

in which q_1, \dots, q_k are arbitrary complex numbers inside the unit disc and k_j some given positive integers. Indeed, the functions $\varphi(x|q)$ satisfy the inversion relation $\varphi(x|q)\varphi(1/x|q) = 1$, hence the contour integrals $\oint G_m G_{m+p}$ are computed exactly like those for F_m , and the norm is unchanged. Note in particular that for $q = 0$, $\varphi(x|q) \propto x$ allows us to multiply $F_m(x)$ by any power of x . This gives us a lot of freedom in picking the model.

Let us now present a simple example, with the same vector space $E = \mathbb{R} \otimes \mathbb{R} \otimes \dots$ we have considered so far.

4.2. Integrable models of discrete 2D Lorentzian gravity with polygonal tiles

Let q_1, q_2, \dots, q_k be generic distinct real numbers with $|q_i| < 1$. Let us introduce the function

$$\phi_m(x|q_1, \dots, q_k) = x \prod_{j=1}^k \frac{(q_j - x)^{m-1}}{(1 - q_j x)^m}, \quad (4.4)$$

for $m = 1, 2, \dots$. We claim that this generates the components of a family of orthogonal vectors $w^{(m)}$ spanning E . The spanning property is clear by noticing that a triangular change of basis maps the canonical one $K_m(x) = x^m$ onto the ϕ_m 's⁹. To see why they are orthogonal, we simply have to compute the following contour integral over the unit disc

$$\oint \frac{dx}{2i\pi x} \phi_m(x|q_1, \dots, q_k) \phi_{m+p}\left(\frac{1}{x}|q_1, \dots, q_k\right) = (-1)^k \oint \frac{dx}{2i\pi} x^{k-1} \prod_{j=1}^k \frac{(1 - q_j x)^{p-1}}{(q_j - x)^{p+1}}, \quad (4.5)$$

⁹ This is true because we assumed the q 's to be generic, i.e. not related by any algebraic relation. It is easy to see for instance in the case $k = 2$, $q_1 = q$, $q_2 = -q$ which is non-generic, that ϕ_m is an odd function of x , in which case only ‘‘half’’ of E is generated.

For $p > 0$, the integrand has no poles outside the unit disc, hence the integral vanishes, and the corresponding vectors are orthogonal. When $p = 0$, we find the normalizations

$$\begin{aligned} N(q_1, \dots, q_k)^{-2} &= \oint \frac{dx}{2i\pi} x^{k-1} \prod_{j=1}^k \frac{1}{(1 - q_j x)(x - q_j)} \\ &= \sum_{j=1}^k \frac{q_j^{k-1}}{1 - q_j^2} \prod_{i \neq j} \frac{1}{(1 - q_i q_j)(q_j - q_i)}, \end{aligned} \quad (4.6)$$

that reproduce the one- q result $N(q) = \sqrt{1 - q^2}$, and give for $k = 2, 3$

$$\begin{aligned} N(q_1, q_2) &= \sqrt{\frac{(1 - q_1^2)(1 - q_2^2)(1 - q_1 q_2)}{1 + q_1 q_2}}, \\ N(q_1, q_2, q_3) &= \sqrt{\frac{(1 - q_1^2)(1 - q_2^2)(1 - q_3^2)(1 - q_1 q_2)(1 - q_1 q_3)(1 - q_2 q_3)}{1 + q_1 q_2 + q_1 q_3 + q_2 q_3 - q_1 q_2 q_3 (q_1 + q_2 + q_3) - (q_1 q_2 q_3)^2}}. \end{aligned} \quad (4.7)$$

The normalizations (4.6) allow us to define orthonormal vectors $v^{(m)} = N(q_1, \dots, q_k) w^{(m)}$, generated by $F_m(x|q_1, \dots, q_k) \equiv N(q_1, \dots, q_k) \phi(x|q_1, \dots, q_k)$. This produces an interesting candidate for the transfer matrix of Lorentzian gravity including triangles, squares, ..., up to $2k + 2$ -gons, with the same fixed staircase boundary conditions as before:

$$\theta_{q_1, \dots, q_k}(x, y|\lambda) = \frac{f_{q_1, \dots, q_k}(\lambda) x y N^2(q_1, \dots, q_k)}{\prod_{i=1}^k (1 - q_i x)(1 - q_i y) - \lambda \prod_{i=1}^k (q_i - x)(q_i - y)}. \quad (4.8)$$

To obtain a well-normalized generating function, we must take f of the form

$$f_{q_1, \dots, q_k}(\lambda) = \frac{g(1 - \lambda(q_1 \dots q_k)^2)}{N^2(q_1, \dots, q_k)}. \quad (4.9)$$

where \sqrt{g} is the Boltzmann weight per boundary triangle, a free parameter of the theory, and the generating function for the transfer matrix elements finally reads

$$\theta_{q_1, \dots, q_k}(x, y|\lambda) = \frac{g x y}{\sum_{i, j=0}^k w_{i, j}(q_1, \dots, q_k|\lambda) x^i y^j}, \quad (4.10)$$

where

$$w_{i, j}(q_1, \dots, q_k|\lambda) = (-1)^{i+j} \frac{\sigma_i \sigma_j - \lambda \sigma_{k-i} \sigma_{k-j}}{\sigma_0^2 - \lambda \sigma_k^2}, \quad (4.11)$$

where the $\sigma_j \equiv \sigma_j(q_1, \dots, q_k)$ are the symmetric functions of the q 's defined by $\prod_{1 \leq j \leq k} (q_j - x) = \sum_{0 \leq i \leq k} (-1)^i \sigma_{k-i} x^i$, with in particular $\sigma_0 = 1$ and $\sigma_k = q_1 q_2 \dots q_k$.

The weights $w_{i,j}$ (4.11) are easily interpreted in terms of different Boltzmann weights for different types of polygons involved in the discrete world-sheet construction. Indeed, following the result of Sect 2.4 in the case of triangles and squares, the coefficients $w_{i,j}$ are the Boltzmann weights of the following local configuration of i lower half-edges merging into j upper ones, all attached to the same point of the time-line:

$$w_{i,j} \leftrightarrow \begin{array}{c} j \\ \diagup \quad \dots \\ \cdot \\ \diagdown \quad \dots \\ i \end{array} \longleftrightarrow \begin{array}{c} j \\ \dots \\ \cdot \\ \dots \\ i \end{array} \quad (4.12)$$

with the obvious dual interpretation as an $(i + j + 2)$ -gonal tile with two time-like edges and i lower- and j upper space-like ones. So the model whose transfer matrix is generated by (4.10) is one of discrete 2D Lorentzian gravity involving polygonal tiles with 3,4,... up to $2k + 2$ edges.

Note that there would be a priori $k(k + 3)/2$ independent coefficients $w_{i,j}$ in the most general symmetric generating function of the form (4.10), whereas here they are expressed in terms of only $k + 1$ independent parameters q_1, \dots, q_k, λ . Hence, we are looking at a rather small-dimensional sub-manifold of the moduli space of 2D Lorentzian gravity, discretized with triangles, squares, ... up to $(2k + 2)$ -gons. The remarkable fact is that this manifold is integrable, as the corresponding transfer matrices commute with one-another. The physical meaning of the particular expression (4.11) for the $w_{i,j}$ weights is however not at all clear. In particular, for more than one q_i , we cannot any longer map the model (as we did in Sect. 2.4 for one q) onto a “generalized curvature model” with only triangles and with additional curvature weights involving now nearest, next-nearest,...up to, say, k 'th-nearest neighbour interactions. Indeed, we can consider the most general model of triangles with a curvature weight a_p for any succession of p up triangles (or p down triangles) and a weight g per triangle (and as before \sqrt{g} for the boundary triangles). The integrable one- q case of Sect. 2 corresponded to the particular choice $a_p = a^{p-1}$. Then it is easy to show that the generating function $\theta(x, y|g, \{a_p\})$ generalizing (2.3) reads

$$\theta(x, y|g, \{a_p\}) = \frac{1}{g} \frac{A(gx)A(gy)}{1 - A(gx)A(gy)}, \quad (4.13)$$

where $A(u) \equiv \sum_{p \geq 1} a_p u^p$ is the generating function for the weights a_p (for the one- q case, we simply had $A(u) = u/(1 - au)$). The particular form (4.13) above then implies that the quantity

$$\frac{g\theta(x, y|g, \{a_p\})}{1 + g\theta(x, y|g, \{a_p\})} = A(gx)A(gy), \quad (4.14)$$

must be factorized into a function of x times the same function of y for some particular g . It is easy to check that for more than one q_i , the generating function $\theta_{q_1, \dots, q_k}(x, y|\lambda)$ given by (4.10) does not satisfy this factorization requirement.

Before we conclude this section, let us slightly extend the definition (4.4) to also include complex (and now non-generic) numbers q_1, \dots, q_k inside the unit disc, but such that ϕ_m remains real. A typical example would be to take $q_1 = q, q_2 = \omega q, q_3 = \omega^2 q, \dots, q_k = \omega^{k-1} q$, where ω is a primitive k -th root of unity. Then we simply have that $\phi_m(x|q_1, \dots, q_k) \propto F_m(x^k|q^k)/x^{k-1}$ with F_m as in (2.6). It is clear that the ϕ_m 's only generate a fraction (roughly $1/k$) of the infinite space E , but the content of the model is exactly the same as that of the one- q one. Another more interesting and possibly generic possibility would be to include both the q 's and their complex conjugates in the list, namely take (4.4) with the $2k$ q 's being $q_1, \dots, q_k, \bar{q}_1, \dots, \bar{q}_k$. Note that the number of free real parameters in that case would still be $2k$. We shall make use of this extension in the next section.

Finally, we can extend the above construction so as to include other boundary conditions. The case of periodic boundary conditions is discussed in detail in Appendix A and corresponds to transfer matrices which are *non-symmetric*. In this case, the construction requires the use of two different (left and right) orthonormal bases.

4.3. Continuum limits

Let us now study the continuum limit of the new models (with k q 's) defined in Sect. 4.2. In this section, we are going to derive the rather negative result that no new scaling behaviour can be obtained from the models of Sect. 4.2, namely that the only well behaved continuum limit leads to the same result as in the one- q case of Sect. 2.6.

To show this, let us first reexamine the case of one q . We start from the generating function (4.8)(4.9) iterated T times:

$$\theta_{q,T}(x, y|\lambda) = (f_q(\lambda))^T \frac{xy(1 - q^2)}{(1 - qx)(1 - qy) - \lambda^T(q - x)(q - y)}, \quad (4.15)$$

with

$$f_q(\lambda) = g \frac{1 - \lambda q^2}{1 - q^2}. \quad (4.16)$$

To get a reasonable continuum limit, after taking $T = \tau/\alpha$ for some small parameter α , we need that both $\lambda = 1 + \mathcal{O}(\alpha)$ and $f_q(\lambda) = 1 + \mathcal{O}(\alpha)$, while g tends to some critical value $g_c < 1$ when $\alpha \rightarrow 0$. From (4.16) above, this is only possible if $q^2 = 1 + \mathcal{O}(\alpha)$ too. So we

assume that q tends to 1^- as $q = e^{-\alpha\sqrt{\Lambda}} = 1 - \alpha\sqrt{\Lambda} + \mathcal{O}(\alpha^2)$. Then from $f_q(\lambda) = 1 + \mathcal{O}(\alpha)$, we deduce at leading order in α that

$$\lim_{\alpha \rightarrow 0} \frac{g_c(1 - \lambda q^2)}{1 - q^2} = 1 \quad \Rightarrow \quad \lambda = 1 - 2\sqrt{\Lambda} \frac{1 - g_c}{g_c} \alpha + \mathcal{O}(\alpha^2). \quad (4.17)$$

Once substituted back into the generating function $\theta_q(x, y|\lambda)$ this gives

$$\lim_{\alpha \rightarrow 0} \theta_q(x, y|\lambda) = \frac{g_c xy}{1 - (1 - g_c)(x + y) + (1 - 2g_c)xy}, \quad (4.18)$$

where we have identified the limiting Boltzmann weights (4.11) in (4.10) as

$$w_{0,0} \rightarrow 1, \quad w_{0,1} = w_{1,0} \rightarrow 1 - g_c, \quad w_{1,1} \rightarrow -(1 - 2g_c), \quad (4.19)$$

which remain all finite in this limit.

Let us now use the same strategy to deal with the k - q model's continuum limit. The T times iterated generating function now reads

$$\theta_{q_1, \dots, q_k; T}(x, y|\lambda) = \frac{(f_{q_1, \dots, q_k}(\lambda))^T xy N^2(q_1, \dots, q_k)}{\prod_{i=1}^k (1 - q_i x)(1 - q_i y) - \lambda^T \prod_{i=1}^k (q_i - x)(q_i - y)}, \quad (4.20)$$

with

$$f_{q_1, \dots, q_k}(\lambda) = g \frac{1 - \lambda(q_1 \dots q_k)^2}{N^2(q_1, \dots, q_k)}, \quad (4.21)$$

as in (4.9) and $N(q_1, \dots, q_k)$ as in (4.6). Setting again $T = \tau/\alpha$ and letting $\alpha \rightarrow 0$ (and $g \rightarrow g_c$, some critical activity per triangle), we must again have both $f_{q_1, \dots, q_k}(\lambda) = 1 + \mathcal{O}(\alpha)$ and $\lambda = 1 + \mathcal{O}(\alpha)$. Let us moreover impose that when $\alpha \rightarrow 0$, all the Boltzmann weights $w_{i,j}$ of (4.11) remain finite. We must then take $N^2(q_1, \dots, q_k) \rightarrow 0$ and therefore $(q_1 \dots q_k)^2 \rightarrow 1$ to be compatible with Eq. (4.21) above. But since all the q 's are real and less than 1 in absolute value, this implies the all $q_i^2 \rightarrow 1$ as $\alpha \rightarrow 0$. Hence the natural generalization of $q = e^{-\alpha\sqrt{\Lambda}}$ to the k - q case reads

$$q_i = \epsilon_i e^{-\alpha_i}, \quad i = 1, 2, \dots, k, \quad (4.22)$$

for some small parameters $\alpha_i > 0$ and some signs $\epsilon_i = \pm 1$. If we now do not impose any longer that the q_i 's are real, we can also choose pairs of conjugate complex numbers

$$q_i = \omega_i e^{-\alpha_i}, \quad \bar{q}_i = \bar{\omega}_i e^{-\alpha_i}, \quad (4.23)$$

with ω_i of modulus 1 and such that $\omega_i^2 \neq 1$.

Our choice is however strongly constrained if we insist in having finite Boltzman weights and it can be checked that, assuming that all the α_i 's are of the same order α , this implies that the norm $N^2(q_1, \dots, q_k)$ itself must be of order α . From the formula (4.7), we see for $k = 2$ and $k = 3$ that this in practice imposes that we can have *at most* one real q_i tending to $+1$ (i.e. $\epsilon_i = +1$ in (4.22) above) and at most one real q_i tending to -1 (i.e. $\epsilon_i = -1$). Finally, to reach a non trivial limit by setting as usual $x = 1 - \alpha X$ and $y = 1 - \alpha Y$, we need *at least* one q_i tending to $+1$. We believe that these requirements are generic for arbitrary k . For $k = 2$, these constraints limit our choice to exactly two real q_i 's as in (4.22) with $\epsilon_1 = +1$ and $\epsilon_2 = -1$. Writing

$$\alpha_i = \alpha \sqrt{\Lambda_i}, \quad i = 1, 2, \quad (4.24)$$

we may easily compute the scaling limit of (4.20) in this case $k = 2$, with $x = 1 - \alpha X$ and $y = 1 - \alpha Y$, and we get

$$\lim_{\alpha \rightarrow 0} \alpha \theta_{q_1, q_2; T}(x, y | \lambda) = \frac{C}{(X + \sqrt{\Lambda_1})(Y + \sqrt{\Lambda_1}) - \phi(X - \sqrt{\Lambda_1})(Y - \sqrt{\Lambda_1})}, \quad (4.25)$$

where $\phi = \lim \lambda^T$, and C is a pre-factor independent of X and Y . This is simply proportional to the one- q result (2.29), and corresponds therefore to the *same* critical behaviour. As mentioned above, the choice

$$q_1 = \omega e^{-\alpha \sqrt{\Lambda}}, \quad q_2 = \bar{\omega} e^{-\alpha \sqrt{\Lambda}}, \quad (4.26)$$

with ω a complex number of modulus 1 and such that $\omega^2 \neq 1$, leads to a trivial limit. Indeed, in this case, $N^2 \sim |1 - \omega^2|^2 \sqrt{\Lambda} \alpha$, and all the Boltzmann weights remain finite, but in the scaling limit where $x = 1 - \alpha X$ and $y = 1 - \alpha Y$, all dependence in X and Y disappears. In fact, as mentioned before, to retain a dependence on X and Y in the scaling limit, we must have at least one q tending to 1, which is not the case here.

Applying now our constraints to the case $k = 3$, we need to choose exactly one of the q_i 's tending to $+1$ and the two others being complex conjugates, i.e.

$$q_1 = e^{-\alpha_1}, \quad q_2 = \omega e^{-\alpha_2}, \quad q_3 = \bar{\omega} e^{-\alpha_2}, \quad (4.27)$$

with again $|\omega| = 1$ and $\omega^2 \neq 1$. The normalization factor now becomes

$$N^2(q_1, q_2, q_3) \sim \frac{2|(1 - \omega)(1 - \omega^2)|^2 \alpha_1 \alpha_2}{2(\alpha_1 + \alpha_2) + (\omega + \bar{\omega})\alpha_2}, \quad (4.28)$$

and we get finite limiting Boltzmann factors by taking

$$\alpha_i = \alpha \sqrt{\Lambda_i}, \quad i = 1, 2. \quad (4.29)$$

Now the scaling limit of (4.20) only retains the factors containing q_1 , and wipes the others out, so we finally get again the form (4.25), with possibly different constants C and ϕ .

We are now ready to treat the general case. Depending on whether k is odd or even, we must take say

$$\begin{aligned} k \text{ odd : } & \quad q_1 = e^{-\alpha_1}, \quad q_{2i} = \omega_i e^{-\alpha_{i+1}}, \quad q_{2i+1} = \bar{\omega}_i e^{-\alpha_{i+1}} \\ & \quad \text{for } i = 1, 2, \dots, (k-1)/2, \\ k \text{ even : } & \quad q_1 = e^{-\alpha_1}, \quad q_2 = -e^{-\alpha_2}, \quad q_{2i+1} = \omega_i e^{-\alpha_{i+2}}, \quad q_{2i+2} = \bar{\omega}_i e^{-\alpha_{i+2}} \\ & \quad \text{for } i = 1, 2, \dots, (k-2)/2, \end{aligned} \quad (4.30)$$

for some generic complex numbers ω_i of modulus 1, and such that $\omega_i^2 \neq 1$. As only one q tends to 1, we are again led to a scaling limit of the form (4.25). Note that in the end of Sect. 4.2 we have already considered the case when $q_j = \omega^{j-1}q$, for $j = 1, \dots, k$ and ω a primitive k -th root of unity, and concluded then that the corresponding model was equivalent to that of $k = 1$, $q_1 = q$ up to some minor rescalings ($x \rightarrow x^k$, $y \rightarrow y^k$, which do not affect the scaling limit): this is in agreement with the present result, for a particular (non-generic) choice of the ω_i 's as k -th roots of unity.

To conclude, all our models have yielded the same and only non-trivial scaling limit for the two-loop correlator as the one- q one of Sect. 2.6. This is a manifestation of the rigidity of our integrability condition, in that all these integrable models share the same universality class.

5. Conclusion

We have revealed an interesting integrability structure underlying the simpler models of two-dimensional Lorentzian quantum gravity and described how one can construct various extensions of these models while keeping them integrable. Among the models considered so far, we have not found any for which the continuum properties of the Lorentzian geometries were different from those of the pure Lorentzian gravity case. We have concentrated on a model of Lorentzian quantum gravity involving a higher curvature term which is equivalent to a model of Lorentzian quantum gravity interacting with a simple dimer

field. The fact that this model has the same continuum behaviour as pure Lorentzian quantum gravity is in contrast with the situation in Euclidean quantum gravity where the introduction of dimers changes the continuum behaviour of the geometrical system [11,19]. On the other hand our results are in compliance with the results of [15], where no interaction was seen when Lorentzian quantum gravity was coupled to an Ising spin system. However, one should bear in mind that when considered as a model describing matter coupled to Lorentzian gravity, our model contains only a subset of the possible matter configurations. It is our hope that our further investigations of the integrability structure revealed will enable us to solve exactly more realistic models of Lorentzian quantum gravity coupled to matter. In the light of the recent results of numerical simulations [16] it would be particularly interesting to study the case of more than two Ising models coupled to Lorentzian quantum gravity. Interpreted as a model involving a higher curvature term our model is similar in spirit to the models considered in [18], where the effect of adding a higher curvature term to usual Euclidean quantum gravity was investigated. The result is the same for Euclidean as for Lorentzian triangulations. Adding a higher curvature term does not change the continuum physics for the geometrical system.

We have furthermore proven the equivalence between Lorentzian triangulations and a certain type of random walks. This equivalence has allowed us to set up a dictionary connecting concepts in Lorentzian quantum gravity to concepts in the theory of random walks. For instance, the loop-loop correlator of pure Lorentzian quantum gravity in the language of random walks became the generating function for large excursions. Furthermore, the integrability structure underlying the triangle-square model of Lorentzian quantum gravity could be understood using a simple block decomposition of the corresponding random walk. Finally, the equivalence between Lorentzian triangulations and random walks has provided us with an explanation why Lorentzian triangulations have fractal dimension two and why the continuum properties of the triangle-square model are the same as those of pure Lorentzian quantum gravity. It is very likely that a further investigation of the random walk picture will likewise tell us under which circumstances, if at all, we can expect new continuum behaviour to occur. We are also convinced that the above mentioned block decomposition will prove useful in revealing the integrability structure underlying the more realistic models of quantum gravity coupled to matter.

Acknowledgements:

P. D. F. thanks the organizers of the semester "Random Matrices and Applications" held at M.S.R.I., Berkeley, for hospitality during the last stage of this work. C. K. thanks Jan Ambjørn for useful discussions.

Appendix A. Non-symmetric transfer matrices and periodic boundary conditions

It is instructive to derive the transfer matrix of the curvature model with periodic boundary conditions. Its features will allow us to enhance dramatically the construction of Sect. 4.2. The transfer matrix for the periodic model with curvature has a marked lower edge (that we will always represent as the leftmost one), and always at least one upper edge, to avoid degeneration into the vacuum. The transfer matrix element $T_{i,j}^{per}(g, a)$ between a row of i lower half-edges and j upper ones reads

$$\begin{aligned}
T_{i,j}^{per}(g, a) &= \sum_{k \geq 1} \sum_{\substack{\Sigma n_r = i, n_1, \dots, n_k \geq 1 \\ \Sigma m_r = j, m_1, \dots, m_{k-1} \geq 1, m_k \geq 0}} \text{Diagram} \\
&= \sum_{k \geq 1} \sum_{\substack{\Sigma n_r = i, n_1, \dots, n_k \geq 1 \\ \Sigma m_r = j, m_1, \dots, m_{k-1} \geq 1, m_k \geq 0}} g^{i+j} a^{\Sigma(n_r-1) + \Sigma(m_r-1) + 2\delta_{m_k,0}} \\
&= (ga)^{i+j} \sum_{k \geq 1} a^{-2k} \binom{i-1}{k-1} \left[\binom{j-1}{k-1} + a^2 \binom{j-1}{k-2} \right],
\end{aligned} \tag{A.1}$$

where the boundary condition is taken into account by the fact that when the rightmost half-edge is a lower one, it receives a weight a as it is the neighbour of the leftmost one, instead of the a^{-1} given by the generic formula a^{m_k-1} at $m_k = 0$. The generating function for (A.1) is readily found to be

$$\begin{aligned}
\theta^{per}(x, y|g, a) &= \sum_{i,j \geq 1} x^i y^j T_{i,j}^{per}(g, a) \\
&= \frac{g^2 xy}{(1-gax)(1-ga(x+y)-g^2(1-a^2)xy)}.
\end{aligned} \tag{A.2}$$

Let us perform the change of parameters $g, a \rightarrow \lambda, q$ of (2.5) and (2.19). The generating function (A.2) is transformed into

$$\begin{aligned}
\theta_q^{per}(x, y|\lambda) &= \frac{q^2(1-\lambda q^2)^2 xy}{((1-qx) - \lambda q(q-x))((1-qx)(1-xy) - \lambda(q-x)(q-y))} \\
&= \lambda \sum_{r,s \geq 1} (1-q^2)^2 \frac{q^{r-1} x(q-x)^{r+s-2}}{(1-qx)^{r+s}} \lambda^{r+s-2} \frac{y(q-y)^{s-1}}{(1-xy)^s} \\
&= \lambda \sum_{m \geq 1} P_m(x|q) \lambda^{m-1} Q_m(y|q).
\end{aligned} \tag{A.3}$$

where

$$\begin{aligned}
P_m(x|q) &= \sqrt{1-q^2} \frac{x(q-x)^{m-1}}{(1-qx)^{m+1}}, \\
Q_m(y|q) &= (1-q^2)^{\frac{3}{2}} \sum_{\substack{r,s \geq 1 \\ r+s=m+1}} q^{r-1} \frac{y(q-y)^{s-1}}{(1-xy)^s} = \sqrt{1-q^2} \left(q^m - \left(\frac{q-y}{1-xy} \right)^m \right).
\end{aligned} \tag{A.4}$$

We know already that the periodic case with curvature is solvable, as we have computed its two-loop correlator above. The reason why is extremely simple: the functions

$$\begin{aligned}
P_m(x|q) &= \sum_{i \geq 1} x^i \bar{w}_i^{(m)}, \\
Q_m(y|q) &= \sum_{j \geq 1} y^j w_j^{(m)},
\end{aligned} \tag{A.5}$$

generate the components of two different left and right vectors $\bar{w}^{(m)}, w^{(m)}$ for T^{per} , that turn out to be orthonormal to one another, i.e. $w^{(m)} \cdot \bar{w}^{(m')} = \delta_{m,m'}$. It is indeed easy to show that the contour integral over the unit circle: $\oint P_m(x|q) Q_{m'}(1/x|q) dx / (2i\pi x) = \delta_{m,m'}$, by use of Cauchy's residue formula.

Note however that these are not eigenvectors of T^{per} but we have the ‘‘diagonal’’ mapping

$$T^{per} \bar{w}^{(m)} = \lambda^m w^{(m)}. \tag{A.6}$$

This translates immediately into the following transfer matrix relation (as before we define $T_q^{per}(\lambda) \equiv T^{per}(g, a)$ with $g, a \rightarrow \lambda, q$)

$$T_q^{per}(\lambda) T_q^{per}(\lambda') = T_q^{per}(\lambda \lambda'). \tag{A.7}$$

Note that this relation is also satisfied by $T_q(\lambda) \otimes T_q(\lambda)$, thanks to (2.23), and justifies a posteriori our previous calculation of the two-loop periodic correlator ($p = 2$ in (2.40)).

Note finally that the two sets of (left and right) vectors span the same space E , as $Q_m(y) \propto y$ for small y , and there is a triangular change of basis from the F_m 's to the P_m 's or Q_m 's.

Let us draw some general conclusion from this example. A score of other models can be constructed by means of two different sets of left and right vectors, provided those are mutually orthonormal. Given any such pair generated by say $P_m(x)$ and $Q_m(y)$, we get a set of transfer matrices $T(\lambda)$ with spectral parameter λ , generated by

$$\theta(x, y|\lambda) = \sum_{i,j \geq 1} T_{i,j}(\lambda) x^i y^j = f(\lambda) \sum_{m \geq 1} P_m(x) \lambda^{m-1} Q_m(y), \quad (\text{A.8})$$

for some arbitrarily chosen function $f(\lambda)$. The vector spaces spanned by the left and right vectors need not be the same, we simply need the vectors to be mutually orthogonal: $\oint dx/(2i\pi x) P_m(x) Q_{m'}(1/x) = \delta_{m,m'}$. This implies a multiplicativity relation

$$T(\lambda)T(\lambda') = \frac{f(\lambda)f(\lambda')}{f(\lambda\lambda')} T(\lambda\lambda'). \quad (\text{A.9})$$

which makes the model trivially integrable.

In the light of this, it is easy to find a non-symmetric generalization of the k q 's model of Sect. 4.2. Taking

$$P_m(x) = M_k x \prod_{j=1}^k \frac{(q_j - x)^{m-1}}{(1 - q_j x)^{m+1}}, \quad (\text{A.10})$$

$$Q_m(y) = (-1)^{k-1} M_k \left((q_1 q_2 \dots q_k)^m - \prod_{j=1}^k \frac{(q_j - y)^m}{(1 - q_j y)^m} \right).$$

as generating functions of the left and right vectors respectively, it is easy to prove that these are mutually orthonormal, provided we take

$$\frac{1}{M_k^2} = (-1)^k \oint \frac{dx}{2i\pi} \prod_{j=1}^k \frac{1}{(1 - q_j x)(q_j - x)}$$

$$= \sum_{j=1}^k \prod_{i=1}^k \frac{1}{1 - q_i q_j} \prod_{\substack{i=1 \\ i \neq j}}^k \frac{1}{q_j - q_i}. \quad (\text{A.11})$$

by Cauchy's formula. For $k = 1$, this gives $M_1 = 1 - q^2$, in agreement with (A.4), while for $k = 2, 3$ we have

$$M_2^2 = \frac{(1 - q_1^2)(1 - q_2^2)(1 - q_1 q_2)}{q_1 + q_2},$$

$$M_3^2 = \frac{(1 - q_1^2)(1 - q_2^2)(1 - q_3^2)(1 - q_1 q_2)(1 - q_2 q_3)(1 - q_1 q_3)}{q_1^2 + q_2^2 + q_3^2 + q_1 q_2 + q_2 q_3 + q_1 q_3 - q_1 q_2 q_3 (q_1 + q_2 + q_3) - q_1^2 q_2^2 - q_2^2 q_3^2 - q_1^2 q_3^2}. \quad (\text{A.12})$$

The vectors (A.10) lead to the transfer matrix generated by (A.8)

$$\begin{aligned} \theta(x, y|\lambda) &= xg(\lambda) \frac{\prod_{j=1}^k q_j(1 - q_j y) - \prod_{j=1}^k (q_j - y)}{\prod_{j=1}^k (1 - q_j x) - \lambda \prod_{j=1}^k q_j(q_j - x)} \times \\ &\quad \times \frac{1}{\prod_{j=1}^k (1 - q_j x)(1 - q_j y) - \lambda \prod_{j=1}^k (q_j - x)(q_j - y)} \end{aligned} \quad (\text{A.13})$$

where $g(\lambda)$ is an arbitrary function of λ (in which we have absorbed various normalization factors). We suspect the transfer matrix of (A.13) to be the periodic boundary condition version of (4.8)(4.9). Note that here the vectors generated by (A.10) both span the same space E (they are proportional to x and y respectively).

Let us finally mention the following generalization of (A.10), based on the general property that if $P_m(x)$ and $Q_m(y)$ are generating functions of mutually orthonormal vectors, then for any function $R(x)$, the vectors generated by $\phi_m(x) = R(x)P_m(x)$ and $\psi_m(y) = Q_m(y)/R(1/y)$ are also mutually orthonormal (we must of course assume that both $R(x)$ and $1/R(1/y)$ have convergent series expansions). We may apply this recipe to (A.10) with the function $R(x) = 1/(\prod_{j=1}^k (1 - q_j x)^{p_j - 1})$, for some given integers $p_j \geq 1$. But $1/R(1/y) = (-1)^{p-k} \prod_{j=1}^k (q_j - y)^{p_j - 1} / y^{p-k}$, where we have defined $p = \sum p_j$, has no good series expansion around $y = 0$. In order to fix this and arrange for both the left and right vectors to generate the same space E as above, we are led to take

$$\begin{aligned} \phi_m(x) &= S_k x \prod_{j=1}^k \frac{(q_j - x)^{m-1}}{(1 - q_j x)^{m+p_j}} \\ \psi_m(y) &= (-1)^p S_k \frac{1}{y^{p-k}} \left(\prod_{j=1}^k \frac{(q_j - y)^{m+p_j-1}}{(1 - q_j y)^m} - \sum_{l=0}^{p-k} \alpha_l y^l \right). \end{aligned} \quad (\text{A.14})$$

The coefficients α_l are fixed by requiring that $\psi_m(y) = O(y)$, and S_k is the normalization factor ensuring orthonormality, with the result $S_k = M_k$ defined in (A.11). Note that for any polynomial P , $P(1/y)$ is automatically orthogonal to $\phi_m(x)$, as no pole lies inside the unit disc in the corresponding Cauchy integral $\oint \phi_m(x) P(x) dx / (2i\pi x) = 0$ for all $m \geq 1$ (the x in the denominator is cancelled by the one in factor of ϕ_m).

References

- [1] H. Kawai, N. Kawamoto, T. Mogami, and Y. Watabiki, Phys.Lett. B306 (1993) 19, hep-th/9302133
- [2] Y. Watabiki, Nucl. Phys. B441 (1995) 119, hep-th/9401096
- [3] J. Ambjørn, and Y. Watabiki, Nucl.Phys. B445 (1995) 129-144, hep-th/9501049
- [4] J. Ambjørn, J. Jurkiewicz and Y. Watabiki, Nucl. Phys. B454 (1995) 313, hep-th/9507014
- [5] J. Ambjørn, K.N. Anagnostopoulos, U. Magnea and G. Thorleifsson, Phys.Lett. B388 (1996) 713-719, hep-lat/9606012
- [6] J. Ambjørn and A.N. Anagnostopoulos, Nucl.Phys. B497 (1997) 445-478, hep-lat/9701006
- [7] J. Ambjørn, P. Bialas and J. Jurkiewicz, JHEP 9902 (1999) 005, hep-lat/9812015
- [8] N. Ishibashi and H. Kawai, Phys. Lett. B322 (1994) 67, hep-th/9312047, Phys. Lett. B352 (1995) 75, hep-th/9503134
- [9] J. Ambjørn, C. Kristjansen and Y. Watabiki, Nucl.Phys. B504 (1997) 555-579, hep-th/9705202
- [10] J. Ambjørn, K.N. Anagnostopoulos, J. Jurkiewicz and C. Kristjansen, JHEP 9804 (1998) 016, hep-th/9802020
- [11] S. Gubser and I. Klebanov, Nucl. Phys. B416 (1994) 827, hep-th/9310098
- [12] J. Ambjørn and R. Loll, Nucl. Phys. B536 (1998) 407, hep-th/9805108
- [13] J. Ambjørn, J. Nielsen, J. Rolf and R. Loll, Chaos Solitons Fractals 10 (1999) 177-195
- [14] R. Nakayama, Phys. Lett. B325 (1994) 347, hep-th/9312158
- [15] J. Ambjørn, K.N. Anagnostopoulos and R. Loll, hep-th/9904012
- [16] J. Ambjørn, private communication
- [17] S. Weinberg, *Ultraviolet divergences in quantum gravity*, in “General Relativity, an Einstein centenary survey” edited by S.W. Hawking and W. Israel, Cambridge University Press 1979
- [18] V. A. Kazakov, M. Staudacher and T. Wynter, Commun. Math. Phys. 179 (1996) 235 (hep-th/9506174), Nucl. Phys. B471 (1996) 309 (hep-th/9601069)
- [19] M. Staudacher, Nucl. Phys. B336 (1990) 349
- [20] Ya.G. Sinai, Theor. Prob. Appl. 27 (1982) 256
- [21] Such expressions for the Sinai model were first derived in A. O. Golosov, Sov. Math. Dokl. 28 (1983) 18. For a more direct derivation based on a real space renormalization group analysis, see P. Le Doussal, C. Monthus and D.S. Fisher, Phys. Rev. E 59 (1999) 4795, cond-mat/9811300. A derivation based on discrete random walks can be found in J. Chave and E. Guitter, J. Phys. A: Math. Gen. 32 (1999) 445, cond-mat/9809087